Polycyclic aromatic hydrocarbons in samples of Ryugu formed in the interstellar medium

Sarah Zeichner, José Aponte, Surjyendu Bhattacharjee, Guannan Dong, Amy Hofmann, Jason Dworkin, Daniel Glavin, Jamie Elsila, Heather Graham, Hiroshi Naraoka, et al.

Title: Isotopic evidence of interstellar-sourced polycyclic aromatic hydrocarbons from Ryugu

Authors: Sarah Zeichner[1*], José C. Aponte[2], Surjyendu Bhattacharjee[1], Guannan Dong[1], Amy E. Hofmann[1,3], Jason P. Dworkin[2], Daniel P. Glavin[2], Jamie E. Elsila[2], Heather V. Graham[2], Hiroshi Naraoka[4], Yoshinori Takano[5], Shogo Tachibana[6,7], Allison T. Karp[8,9,10], Kliti Grice[11], Alex I. Holman[11], Katherine H. Freeman[8], Hisayoshi Yurimoto[12], Tomoki Nakamura[13], Takaaki Noguchi[14], Ryuji Okazaki[4], Hikaru Yabuta[15], Kanako Sakamoto[7], Toru Yada[7], Masahiro Nishimura[7], Aiko Nakato[7], Akiko Miyazaki[7], Kasumi Yogata[7], Masanao Abe[7,16] Tatsuaki Okada[6,7], Tomohiro Usui[6,7], Makoto Yoshikawa[7,16] Takanao Saiki[7], Satoshi Tanaka[7,16] Fuyuto Terui [17], Satoru Nakazawa[7], Sei-ichiro Watanabe[18], Yuichi Tsuda[7], Kenji Hamase[4], Kazuhiko Fukushima[18], Dan Aoki[18], Minako Hashiguchi[18], Hajime Mita[19], Yoshito Chikaraishi[12], Naohiko Ohkouchi[5], Nanako O. Ogawa[5], Saburo Sakai[5], Eric T. Parker[2], Hannah L. McLain[2], Francois-Regis Orthous-Daunay[20], Véronique Vuitton[20], Roland Thissen[22], Cédric Wolters[20], Philippe Schmitt-Kopplin[21], Alexander Ruf[23] , Junko Isa[28], Norbert Hertkorn[21], Yasuhiro Oba[12], Toshiki Koga[5], Toshihiro Yoshimura[5], Daisuke Araoka[24], Haruna Sugahara[7], Aogu Furusho[4], Kazunori Sasaki[25], Hajime Sato[25], Yoshihiro Furukawa[13], Junken Aoki[6], Kuniyuki Kano[6], Shin-ichiro M. Nomura[13], Takaaki Yoshikawa[26], Satoru Tanaka[26], Mayu Morita[26], Morihiko Onose[26], Fumie Kabashima[27], Kosuke Fujishima[28], Tomoya Yamazaki[12], Yuki Kimura[12], John M. Eiler[1]

Affiliations:

[1] Geological and Planetary Science Division, California Institute of Technology, Pasadena, CA 91125

[2] Solar System Exploration Division, NASA Goddard Space Flight Center, Greenbelt, MD 20771, USA

[3] Jet Propulsion Laboratory, California Institute of Technology, Pasadena, CA 91109, USA

[4] Kyushu University, Fukuoka 819-0395, Japan

[5] Japanese Agency for Marine-Earth Science and Technology (JAMSTEC), Yokosuka, Kanagawa, 237-0061, Japan

[6] University of Tokyo, 7-3-1 Hongo, Tokyo 113-0033, Japan

[7] Institute of Space and Astronautical Science (ISAS), Japan Aerospace Exploration Agency (JAXA), Sagamihara 252-5210, Japan

[8] Department of Geosciences, The Pennsylvania State University, University Park, PA 16802, USA

[9] Ecology and Evolutionary Biology Department, Yale University, New Haven, CT, USA
[10] Department of Environmental, Earth, and Planetary Sciences, Brown University, Providence, RI, USA
[11] WA Organic & Isotope Geochemistry Centre, The Institute for Geoscience Research, School of Earth and Planetary Sciences, Curtin University, Bentley, WA 6102, Australia

[12] Hokkaido University, Sapporo 060-0810, Japan
[13] Tohoku University, Sendai 980-8578, Japan
[14] Kyoto University, Kyoto 606-8502, Japan

[15] Hiroshima University, Higashi-Hiroshima 739-8526, Japan
[16] School of Physical Sciences, The Graduate University for Advanced Studies, Hayama 240-0193, Japan.
[17] Department of Mechanical Engineering, Kanagawa Institute of Technology, Atsugi 243-0292, Japan.

[18]Nagoya University, Nagoya 464-8601, Japan.

[19]Fukuoka Institute of Technology, Fukuoka 811-0295, Japan

[20]Université Grenoble Alpes, 621 Av. Centrale, 38400 Saint-Martin-d'Hères, France.

[21]Helmholtz Zentrum München, Analytical BioGeoChemistry, Ingolstaedter

Landstraße 1, 85764 Neuherberg, Germany

[22] LaboratoireChimiePhysique, Centre National Recherche Scientifique (CNRS), University of Paris-Sud, Orsay, France
[23]CNRS, Laboratoire de Physique des Interactions Ioniques et Moléculaires, Université Aix- Marseille, 13397 Marseille, France.

[24] Geological Survey of Japan, National Institute of Advanced Industrial Science and Technology (AIST), Tsukuba, Ibaraki 305-8567, Japan

[25]Human Metabolome Technologies Inc., Kakuganji, Tsuruoka, Yamagata, 997-0052, Japan

[26]Analytical Technology Division, Horiba Techno Service Co. Ltd., Kyoto 601-8125, Japan.

[27]LECO Japan Corporation, 2-13-4 Shiba, Minato-ku, Tokyo 105-0014, Japan

[28]Earth-Life Science Institute, Tokyo Institute of Technology, Tokyo 1528550, Japan

*Corresponding author; szeichner@caltech.edu

Abstract: Polycyclic aromatic hydrocarbons (PAHs) are a class of molecules constituting up to 20% of elemental carbon in our Galaxy. They are potentially produced within circumstellar environments (≳1000K), by shock wave breakdown or chemical re-processing of carbon-rich grains in nebular or asteroidal settings, or by reactions within the cold (~10K) interstellar medium. We measured isotopic properties of PAHs extracted from Ryugu asteroid and Murchison meteorite, finding doubly-^{13}C substituted compositions of naphthalene, fluoranthene, and pyrene to be 10-65‰ higher than the expected stochastic distribution. This exceeds isotopic fractionations associated with high-temperature chemical processes, but is consistent with formation of PAH formation in the interstellar medium. Ryugu phenanthrene and anthracene have approximately stochastic doubly-^{13}C-substituted compositions, suggesting formation dominated by components made by higher-temperature chemistry.

One-Sentence Summary: Large fraction of polycyclic aromatic hydrocarbons in Ryugu and Murchison derives from cold interstellar molecular clouds

Main Text

Polycyclic aromatic hydrocarbons (PAHs) are ubiquitous, with abundances ~10^{-7} times the abundance of hydrogen (*1*), and constituting up to 20% of the elemental carbon budget of our Galaxy (*1–3*) and other galaxies (e.g., (*4*)). PAHs may serve as building blocks for the aromatic carbon-rich grains abundant within interstellar environments (*5*) and higher molecular weight insoluble organic material (IOM) that comprises most of the carbon within meteorites (*6*). However, we do not currently understand the dominant processes that produce these forms of reduced carbon in extraterrestrial settings (Fig. 1; (*7*)).

Smaller aromatic organics (i.e., PAHs of a few rings) can form through radical growth reactions in the gas phase (e.g., hydrogen-abstraction-carbon-addition reaction mechanism or "HACA"; (*7*)) in hot circumstellar environments (>1000K around C-rich Asymptotic Giant Branch (AGB) stars; Fig. 1). C-rich grains and IOM potentially may be constructed via similar processes. These high-temperature mechanisms are thought to be relatively inefficient and a complete model for synthesis in the outflows of AGB stars is lacking (*7*).

Alternatively, PAHs could form in the cold interstellar medium (ISM; ~10K) through barrierless reactions (Fig. 1, (*7–12*)). Laboratory experiments have characterized relevant chemical mechanisms, but empirical evidence for PAH formation in the ISM is limited; to date, only (*13*) and (*14*) have identified nitriles inferred to be derived from PAHs—benzo-nitrile and cyanonaphthalenes, respectively—within molecular clouds.

Finally, PAHs can be formed from the destruction of carbon-rich grains by shock wave breakdown, cosmic rays or UV photolysis (*15*), but can also be destroyed by these same processes (Fig. 1). The time scales for the destruction of PAHs by these mechanisms (*16*, *17*) are shorter than the time scales of PAH ejection from circumstellar envelopes of AGB stars (*9*, *18*), making it unlikely that circumstellar synthesis dominates the formation of extraterrestrial PAHs; evidence for interstellar formation of extraterrestrial PAHs may resolve this paradox in the Galaxy's carbon budget.

The study of soluble PAHs and IOM within carbonaceous chondrite meteorites (CCs) and samples returned by collection missions to asteroids presents an opportunity to further elucidate how these compounds are formed. Here, compound-specific isotope analyses of PAHs extracted from Ryugu samples, and comparison with similar measurements of PAHs from a primitive CC, offer an unprecedented opportunity to constrain the synthesis mechanisms of extraterrestrial

PAHs in a sample that has never experienced unsupervised exposure to the terrestrial environment.

Isotope analysis

Rare-isotope distributions constrain the source, substrates, and chemical mechanisms responsible for forming organic molecules (*19*, *20*). The molecular-average ratios of $^{13}C/^{12}C$ and D/H of meteoritic organics (reported as $\delta^{13}C_{VPDB}$ and δD_{VSMOW}, respectively; (*21*)) are often outside the ranges of ratios measured in terrestrial organics — observations often cited as evidence of the inheritance of atoms from ISM precursors (*22*, *23*). More specifically, ^{13}C enrichment of some extraterrestrial organics, such as aldehydes and amino acids (*24*), are interpreted as products of precursors deriving from a very ^{13}C-enriched CO pool. In contrast, PAHs are thought to be formed from the more-^{13}C-deplete, reduced interstellar C pool (*7*), leading to products with lower carbon isotope values than those formed from CO and without this diagnostic heavy "interstellar fingerprint." However, heterogeneities in the carbon isotopic composition of interstellar C make these arguments uncertain and multiple distinct processes can contribute to similar molecular-average $\delta^{13}C$ and δD values, which can lead to non-unique interpretations of their origins.

Multiple-substitutions ("clumping") of heavy isotopes within molecules reflect temperature-dependent chemical reactions and physical processes (*19*), further constraining molecular origins. For given molecular-average $\delta^{13}C$ values of extraterrestrial PAHs, a small proportion of each molecule is doubly-^{13}C substituted ('$2x^{13}C$'). Abundances of clumped ^{13}C isotopologues are reported as differences, or $\Delta 2x^{13}C$ values, between of doubly-^{13}C-substituted to unsubstituted isotopologues of a sample and that same ratio expected in that sample if it possessed a ratio equal to the stochastic probability of a double substitution based on its molecular-average ^{13}C abundance.

Variations in $2x^{13}C$ clumping can be temperature-dependent because heavy isotopic substitution lowers the molecular vibrational energy of, and therefore stabilizes, the C-C bond, thus making isotopologue clumping increasingly favorable at lower temperatures. Acetylene is an ideal model to understand $2x^{13}C$ clumping, as it is commonly invoked as the precursor to the formation of interstellar aromatic reduced carbon (*25*) including PAHs (*26*, *27*), where hydrocarbon frames could be built via ion-neutral reactions between C+ and CH_n in the gas phase of molecular clouds (*28*, *29*). The equilibrium exchange reaction between single and double-^{13}C substitution in acetylene —

$$2 * {}^{13}C{}^{12}CH_2 \rightleftharpoons {}^{13}C_2H_2 + {}^{12}C_2H_2 \ (Eqn.\ 1)$$

(Fig. 2D; Fig. S5&6; (*21*); similar arguments would apply for other small C2 and C3 precursors of PAHs) — is driven to the right at all temperatures, resulting in enrichments in $\Delta 2x^{13}C$ of 10s of per-mille (‰) at temperatures of 10-50K typical of the ISM (*10*) and negligible $\Delta 2x^{13}C$ values at circumstellar temperatures or temperatures typical of aqueous alteration in meteorite parent bodies (Fig. 2D, 3A&B; Fig. S6). We note that chemical kinetic isotope effects produced by irreversible reactions typically have amplitudes of clumped isotope Δ indices similar to those of equilibrium isotope effects (*20*), but could be positive or negative. We expect that PAHs formed in the cold ISM should have $\Delta 2x^{13}C$ values substantially different from zero (and necessarily positive if formed by reversible reactions), while PAHs formed in hot circumstellar envelopes ($\gtrsim$1000 K for AGB stars) should have $\Delta 2x^{13}C$ approaching zero.

PAHs from Ryugu, Murchison and combusted plant biomass

The Hayabusa2 mission collected 5.4 g of sample from two locations on near-Earth carbonaceous asteroid (1623173) Ryugu (*30*), which has been demonstrated to be compositionally similar to Ivuna (CI)-type meteorites (*31*). The soluble organic molecules team prepared solvent extracts of Ryugu samples A0106 and C0107 (aggregates of sub-mm grains collected from the first and second touchdowns, respectively; Fig S1; (*24*, *32*)). Endogenous, complex soluble aromatic organics were identified in analyses of the dichloromethane (DCM) extract at NASA Goddard Space Flight Center. Among these, 2-, 3- and 4-ring PAHs naphthalene, phenanthrene, anthracene, fluoranthene, and pyrene were identified (Fig. 1&Sl), but their abundances were below the necessary amounts for isotopic analysis via traditional GC-combustion isotopic ratio mass spectrometry (IRMS; 8.6-32.4 nmol/g; (*24*, *32*)).

We analyzed PAHs within DCM extracts of Ryugu samples A0106 and C0107 using gas chromatography (GC)-Orbitrap mass spectrometry (*33*). We measured the $\delta^{13}C$ values of these five PAHs extracted from Hayabusa2 sample A0106; $\delta^{13}C$, δD and $\Delta 2x^{13}C$ values of these five PAHs from C0107; and $\delta^{13}C$ and $\Delta 2x^{13}C$ values of fluoranthene and pyrene from another carbonaceous chondrite—Murchison ((*33*); Table 1; Fig 2; Fig. S3A&B). The $\delta^{13}C$ values of Ryugu PAHs measured here are generally higher than the $\delta^{13}C$ values of terrestrial PAHs and in some cases consistent within error with past measurements of $\delta^{13}C$ values of meteorite-extracted PAHs (Fig. S4). $\delta^{13}C$ values of fluoranthene and pyrene from Murchison were consistent with past measurements of the same compounds by traditional GC-isotope-ratio-mass-spectrometry (e.g., (*34*)). PAHs were not observed in quantities above background within the serpentine blank prepared in parallel with the Ryugu samples (Table S1).

We also measured $\delta^{13}C$ and $\Delta 2x^{13}C$ values of combusted plant biomass to constrain double-^{13}C substitutions in PAHs formed by high temperature soot-forming chemistries. We did not measure δD and $\Delta 2x^{13}C$ values of PAHs from A0106 and δD values from Murchison or combustion-produced PAHs (*21*).

Cold PAH formation

The elevated $\Delta 2x^{13}C$ values of 9-51‰ for naphthalene, fluoranthene and pyrene from Ryugu and fluoranthene from Murchison exceed the predicted stochastic values (p-values < 0.005; (*21*)). The magnitude of the observed $\Delta 2x^{13}C$ anomalies is unusual; a previous study of common physical and chemical fractionations at Earth-surface conditions demonstrated subtle variations (~1‰) in the $2x^{13}C$-compositions of ethane (*35*); while additional measurements of this relatively new isotopic property must be done to fully constrain compositions of terrestrial organics, variations of ~1‰ are expected for most easily envisioned chemical, biological and physical processes.

The large positive $\Delta 2x^{13}C$ anomalies we observe in most Ryugu and Murchison PAHs are consistent with the hypothesis that some percentage of these compounds were synthesized within cold (<50 K) environments (Fig. 3A&B) via a process that preferentially formed excesses of ^{13}C-^{13}C bonds but progressed with high yield, such that the overall ^{13}C abundances of the products approached those of the reactant pool. This latter conclusion is supported by our result that the clumped-^{13}C composition is independent of molecular-average $\delta^{13}C$ values (which are similar within error for even and odd ring number PAHs in Ryugu, and between fluoranthene and pyrene in Murchison).

The highest $\Delta 2x^{13}C$ value we observe, 51±13‰ for Murchison fluoranthene, is close to the acetylene equilibrium value at ~10K, suggesting that most of the fluoranthene in this sample was synthesized in the ISM (*10*). Further, this suggests that the low-temperature reactions preferentially forming $2x^{13}C$ clumps not only occur in the initial formation of C-C bonds, but also in the assembly of high-molecular-weight aromatic compounds from those smaller substrates (i.e., as otherwise assembly of larger structures would dilute the initial signature of smaller precursors). This $\Delta 2x^{13}C$ value is higher than those of the 2- and 4-ring PAHs from Ryugu, whose positive but lower $\Delta 2x^{13}C$ values are consistent with any of following three scenarios: first, Ryugu 2- and 4-ring PAHs may have formed at higher temperatures than Murchison's fluoranthene (20-50K). Second, Ryugu 2- and 4-ring PAHs might be mixtures of two or more end-member sources, with 20-50% formed in cold interstellar environments and the rest formed or reprocessed at higher temperatures within circumstellar, nebular or asteroidal environments. Finally, they could have formed at low ISM temperatures from 2- or 3-carbon precursors with large positive $\Delta 2x^{13}C$ values, and then converted into larger, aromatic molecules through reactions that diluted the initial $\Delta 2x^{13}C$ signature.

Hot PAH formation

Synthesis of PAHs at high-temperature is not expected to produce $\Delta 2x^{13}C$ values distinguishable from zero by the analytical methods used in this study (*21*). Indeed, we observed no statistically significant deviations from the expected stochastic distributions of doubly-^{13}C-substituted species in PAHs extracted from combusted plant biomass (p-values > 0.04; Figure 2; Table S3; (*21*)), supporting our expectation that PAHs formed at high temperatures are not associated with 10's-of-per-mille clumped isotope anomalies.

Three extraterrestrial PAH samples examined in this study have $\Delta 2x^{13}C$ values that are near-stochastic (p-values > 0.15; (*21*)): phenanthrene and anthracene from Ryugu and pyrene from Murchison. High-temperature processes capable of de-novo formation of 3-ring PAHs from Ryugu and pyrene from Murchison include: condensation in the outflows of C-rich AGB stars through either "bottom-up" synthesis (e.g., hydrogen-abstraction-carbon-addition ("HACA") mechanism) or "top-down" catagenetic breakdown of larger carbonaceous grains. A computational study of HACA formation of PAHs predicted the formation of 3-ring PAHs phenanthrene and anthracene in excess (as compared to other ring sizes of PAHs), potentially linked to the conversion of acenaphthalene to the phenanthryl radical (*36*). Thus, PAHs formed via HACA could dominate the 3-ring species while contributing less to the quantity of other PAH species. A complete understanding of the formation of 3-ring PAHs in extraterrestrial environments is still lacking but has been recently advanced by both experimental and theoretical studies (e.g., (*37*)).

In Ryugu, molecular-average δD values of the 3-ring PAHs were systematically lower compared to those of the 2- and 4-ring PAHs. We expect that the formation of aromatic compounds by HACA chemistry in stellar envelopes would produce compounds with high $\delta^{13}C$ and low δD values following the burning of deuterium within the star's core (Fig. 3A; (*38*)), which is consistent with data observed for Ryugu phenanthrene and anthracene. Paired compound-specific $\Delta 2x^{13}C$ and δD data for Murchison PAHs would be required to provide additional insights for that specimen.

Contributions from PAHs formed in the parent body

Isotopic compositions of PAHs may reflect variable dilution, and/or destruction and replacement, of an original population formed in the ISM (and, as shown here, possibly having high $\Delta 2x^{13}C$) by a secondary population of PAHs that were generated in the parent body from existing carbon sources at moderate temperature, but still having near-stochastic $\Delta 2x^{13}C$. Potential PAH-forming reactions associated with secondary processing in a nebulary or parent body environment include FTT synthesis from CO, reactive dissolved inorganic carbon (DIC), or other substrates (along with subsequent reactions among hydrocarbon products, i.e., aromatization), or the catagenetic breakdown of larger macromolecular carbon (which is aromatic and highly abundant in carbonaceous chondrites). While aromatization of FTT synthesis products is unlikely to occur at temperatures experienced by Ryugu's parent body (no higher than 200°C; (*39*)), previous pyrolysis experiments on meteoritic IOM have demonstrated the formation of 2-, 3-, and 4-ring PAHs observed in A0106 and C0107 at plausible parent body temperatures (*40*). If the proportions of PAHs generated by secondary processes differ from those generated via primary ISM synthesis, then mixing of the former with the latter could lead to mixtures in which some compounds (i.e., those made in relatively great abundance in parent body processes) have near-stochastic clumped isotope compositions while other co-existing PAH's (those that were formed in greater relative abundances in the ISM) retain large positive $\Delta 2x^{13}C$ anomalies.

This hypothesis is independently supported by PAH δD values and their correlation with $\Delta 2x^{13}C$ values, along with molecular properties and host-rock histories of the Ryugu asteroid and Murchison meteorite (Figs. 2D and 3A). PAHs formed in the parent body are expected to have low δD_{VSMOW} values, like the values measured for phenanthrene and anthracene from Ryugu (Fig. 3A; (*41*)). Hydrogen of PAHs that were formed by primary interstellar processes can also exchange and equilibrate with parent body water (*42*), which is deuterium-depleted (δD_{VSMOW} ~ -440‰ based on prior studies of CCs, including Murchison; (*43*)). The exact δD value of Ryugu parent body water has yet to be characterized. Carbon-rich grains in Ryugu samples have been demonstrated to be heterogeneous in their δD values, ranging from very low values (-1000; i.e., no D detected) to hotspots of 10,000‰ (*39*), suggesting that parent body alteration processes did not pervasively equilibrate or homogenize hydrogen isotopic distributions in Ryugu samples. However, some exchange of D between PAHs and parent body water is possible, particularly given Ryugu's characterization as being petrologically similar to a CI-type chondrite (*31*). It is not obvious whether the carbon isotopes of PAHs can exchange, directly or indirectly, between PAHs and the co-existing reactive carbon source under parent body conditions. However, formation of new PAH's from parent body substrates (water, dissolved inorganic carbon, or DIC) would drive the $\delta^{13}C$ values of the combined mixture of PAHs towards the composition of dissolved inorganic carbon in primitive bodies (Murchison carbonate has $\delta^{13}C$ of +20 to 80‰; Fig. 3A).

Formation of PAHs via synthesis in the parent body also offers a potential interpretation for the differences between the $\Delta 2x^{13}C$ values of fluoranthene and pyrene from Murchison. Although CM2 carbonaceous chondrites are broadly less aqueously altered than CI-type chondrites, Murchison has a known history of aqueous alteration and organic matter reprocessing (*44*), which can be variable even for different chips of the same specimen (*45*). Our data demonstrates that the metastable isomer—fluoranthene (*46*)— preserves a large $\Delta 2x^{13}C$ value of 51‰ consistent with preferential ^{13}C-clumping at cold interstellar temperatures, while the more stable isomer—pyrene (*46*)—has $\Delta 2x^{13}C$ values near the stochastic distribution. Any formation of PAHs under parent body conditions would be expected to more closely approach

thermodynamic, including isotopic, equilibrium that favors more stable isomers (*47*)—pyrene, in this case—which upon mixing with pre-existing PAHs formed via other pathways, would dilute and potentially erase any original interstellar anomalies in intramolecular isotopic structure (i.e., $2x^{13}C$ clumping).

Final thoughts

The diversity in isotopic signatures of PAH's from Ryugu and Murchison are consistent with them being a mixture of at least two end member components (*21, 48*): one that was synthesized in cold interstellar environments, and a second that was relatively rich in 3-ring species and synthesized or reprocessed in high-temperature settings. This work is one of the first to measure multiply-substituted isotopic forms of reduced carbon from cosmochemical settings, and the first to do so on a returned sample. Our conclusion—a large fraction of extraterrestrial PAHs are formed by interstellar processes—is justified by first-order understanding of chemical isotope effects, the isotopic compositions of components of meteorite samples, and prior studies of interstellar and circumstellar chemistry. Our measurements provide insights into PAH formation processes, offering quantitative support for a central question within astrochemistry: how does extraterrestrial aromatic carbon form?

References and Notes

1. A. G. G. M. Tielens, The molecular universe. *Rev Mod Phys*. **85**, 1021–1081 (2013).
2. L. J. Allamandola, S. A. Sandford, B. Wopenka, Interstellar Polycyclic Aromatic Hydrocarbons and Carbon in Interplanetary Dust Particles and Meteorites. *Science (1979)*. **237**, 56–59 (1987).
3. A. Léger, L. d'Hendecourt, D. Defourneau, Physics of IR emission by interstellar PAH molecules. *Astron Astrophys*. **216**, 148–164 (1989).
4. J. D. T. Smith, B. T. Draine, D. A. Dale, J. Moustakas, Jr. , R. C. Kennicutt, G. Helou, L. Armus, H. Roussel, K. Sheth, G. J. Bendo, B. A. Buckalew, D. Calzetti, C. W. Engelbracht, K. D. Gordon, D. J. Hollenbach, A. Li, S. Malhotra, E. J. Murphy, F. Walter, The Mid- Infrared Spectrum of Star- forming Galaxies: Global Properties of Polycyclic Aromatic Hydrocarbon Emission. *Astrophys J*. **656**, 770–791 (2007).
5. B. T. Draine, Graphite Revisited. *Astrophys J*. **831**, 109 (2016).
6. A. G. G. M. Tielens, Interstellar polycyclic aromatic hydrocarbon molecules. *Annu Rev Astron Astrophys*. **46**, 289–337 (2008).
7. R. I. Kaiser, N. Hansen, An Aromatic Universe-A Physical Chemistry Perspective. *Journal of Physical Chemistry A*. **125** (2021), pp. 3826–3840.
8. R. I. Kaiser, D. S. N. Parker, A. M. Mebel, Reaction dynamics in astrochemistry: Low-temperature pathways to polycyclic aromatic hydrocarbons in the interstellar medium. *Annu Rev Phys Chem*. **66**, 43–67 (2015).
9. S. Doddipatla, G. R. Galimova, H. Wei, A. M. Thomas, C. He, Z. Yang, A. N. Morozov, C. N. Shingledecker, A. M. Mebel, R. I. Kaiser, Low-temperature gas-phase formation of indene in the interstellar medium. *Sciences Advances*. **7** (2020).
10. K. I. Öberg, Photochemistry and Astrochemistry: Photochemical Pathways to Interstellar Complex Organic Molecules. *Chem Rev*. **116**, 9631–9663 (2016).
11. A. M. Burkhardt, R. A. Loomis, C. N. Shingledecker, K. L. K. Lee, A. J. Remijan, M. C. McCarthy, B. A. McGuire, Ubiquitous aromatic carbon chemistry at the earliest stages of star formation. *Nat Astron*. **5**, 181–187 (2021).

12. M. C. Mccarthy, B. A. Mcguire, Aromatics and Cyclic Molecules in Molecular Clouds: A New Dimension of Interstellar Organic Chemistry. *Journal of Physical Chemistry A*. **125**, 3231–3243 (2021).
13. B. A. McGuire, A. M. Burkhardt, S. Kalenskii, C. N. Shingledecker, A. Remijan, E. Herbst, M. McCarthy, Detection of the aromatic molecule benzonitrile (c-C6H5CN) in the interstellar medium. *Science (1979)*. **359**, 202–205 (2018).
14. B. A. McGuire, R. A. Loomis, A. M. Burkhardt, K. Long Kelvin Lee, C. N. Shingledecker, S. B. Charnley, I. R. Cooke, M. A. Cordiner, E. Herbst, S. Kalenskii, M. A. Siebert, E. R. Willis, C. Xue, A. J. Remijan, M. C. McCarthy, Detection of two interstellar polycyclic aromatic hydrocarbons via spectral matched filtering. *Science (1979)*. **371**, 1265–1269 (2021).
15. J. E. Chiar, A. G. G. M. Tielens, A. J. Adamson, A. Ricca, The structure, origin, and evolution of interstellar hydrocarbon grains. *Astrophysical Journal*. **770** (2013), doi:10.1088/0004-637X/770/1/78.
16. E. R. Micelotta, A. P. Jones, A. G. G. M. Tielens, Polycyclic aromatic hydrocarbon processing in interstellar shocks. *Astron Astrophys*. **510**, 1–19 (2010).
17. E. R. Micelotta, A. P. Jones, A. G. G. M. Tielens, Polycyclic aromatic hydrocarbon processing in a hot gas. *Astron Astrophys*. **510**, A37 (2010).
18. M. Frenklach, E. D. Feigelson, Formation of polycyclic aromatic hydrocarbons in circumstellar envelopes. *Astrophys J*. **341**, 372–384 (1989).
19. J. M. Eiler, The Isotopic Anatomies of Molecules and Minerals. *Annu Rev Earth Planet Sci*. **41**, 411–441 (2013).
20. J. Bigeleisen, M. Wolfsberg, Theoretical and experimental aspects of isotope effects in chemical kinetics. *Adv Chem Phys*. **1**, 15–76 (1957).
21. Materials and methods are available as supplementary materials.
22. D. P. Glavin, C. M. Alexander, J. C. Aponte, J. P. Dworkin, J. E. Elsila, H. Yabuta, *The origin and evolution of organic matter in carbonaceous chondrites and links to their parent bodies* (Elsevier, 2018; https://linkinghub.elsevier.com/retrieve/pii/B9780128133255000033).
23. J. E. Elsila, S. B. Charnley, A. S. Burton, D. P. Glavin, J. P. Dworkin, Compound-specific carbon, nitrogen, and hydrogen isotopic ratios for amino acids in CM and CR chondrites and their use in evaluating potential formation pathways. *Meteorit Planet Sci*. **47**, 1517–1536 (2012).
24. H. Naraoka, Y. Takano, J. P. Dworkin, Y. Oba, K. Hamase, A. Furusho, N. O. Ogawa, M. Hashiguchi, K. Fukushima, D. Aoki, P. Schmitt-Kopplin, J. C. Aponte, E. T. Parker, D. P. Glavin, H. L. McLain, J. E. Elsila, H. V. Graham, J. M. Eiler, F.-R. Orthous-Daunay, C. Wolters, J. Isa, V. Vuitton, R. Thissen, S. Sakai, T. Yoshimura, T. Koga, N. Ohkouchi, Y. Chikaraishi, H. Sugahara, H. Mita, Y. Furukawa, N. Hertkorn, A. Ruf, H. Yurimoto, T. Nakamura, T. Noguchi, R. Okazaki, H. Yabuta, K. Sakamoto, S. Tachibana, H. C. Connolly, D. S. Lauretta, M. Abe, T. Yada, M. Nishimura, K. Yogata, A. Nakato, M. Yoshitake, A. Suzuki, A. Miyazaki, S. Furuya, K. Hatakeda, H. Soejima, Y. Hitomi, K. Kumagai, T. Usui, T. Hayashi, D. Yamamoto, R. Fukai, K. Kitazato, S. Sugita, N. Namiki, M. Arakawa, H. Ikeda, M. Ishiguro, N. Hirata, K. Wada, Y. Ishihara, R. Noguchi, T. Morota, N. Sakatani, K. Matsumoto, H. Senshu, R. Honda, E. Tatsumi, Y. Yokota, C. Honda, T. Michikami, M. Matsuoka, A. Miura, H. Noda, T. Yamada, K. Yoshihara, K. Kawahara, M. Ozaki, Y. Iijima, H. Yano, M. Hayakawa, T. Iwata, R. Tsukizaki, H.

Sawada, S. Hosoda, K. Ogawa, C. Okamoto, N. Hirata, K. Shirai, Y. Shimaki, M. Yamada, T. Okada, Y. Yamamoto, H. Takeuchi, A. Fujii, Y. Takei, K. Yoshikawa, Y. Mimasu, G. Ono, N. Ogawa, S. Kikuchi, S. Nakazawa, F. Terui, S. Tanaka, T. Saiki, M. Yoshikawa, S. Watanabe, Y. Tsuda, Soluble organic molecules in samples of the carbonaceous asteroid (162173) Ryugu. *Science (1979)*. **379** (2023), doi:10.1126/science.abn9033.

25. F. Lahuis, E. F. van Dishoeck, "ISO-SWS spectroscopy of gas-phase C 2 H 2 and HCN toward massive young stellar objects" (2000).
26. M. J. Abplanalp, R. I. Kaiser, Implications for Extraterrestrial Hydrocarbon Chemistry: Analysis of Acetylene (C 2 H 2) and D2-acetylene (C 2 D 2) Ices Exposed to Ionizing Radiation via Ultraviolet–Visible Spectroscopy, Infrared Spectroscopy, and Reflectron Time-of-flight Mass Spect. *Astrophys J.* **889**, 3 (2020).
27. A. M. Mebel, A. Landera, R. I. Kaiser, Formation Mechanisms of Naphthalene and Indene: From the Interstellar Medium to Combustion Flames. *Journal of Physical Chemistry A.* **121**, 901–926 (2017).
28. O. Martinez, N. B. Betts, S. M. Villano, N. Eyet, T. P. Snow, V. M. Bierbaum, Gas Phase Study of C + Reactions of Interstellar Relevance. *Astrophys J.* **686**, 1486–1492 (2008).
29. S. S. Prasad, W. T. Huntress, A model for gas phase chemistry in interstellar clouds: I. The basic model, library of chemical reactions, and chemistry among C, N and O compounds. *Astrophys J Suppl Ser*. **43**, 1–35 (1980).
30. S. Tachibana, H. Sawada, R. Okazaki, Y. Takano, K. Sakamoto, Y. N. Miura, C. Okamoto, H. Yano, S. Yamanouchi, P. Michel, Y. Zhang, S. Schwartz, F. Thuillet, H. Yurimoto, T. Nakamura, T. Noguchi, H. Yabuta, H. Naraoka, A. Tsuchiyama, N. Imae, K. Kurosawa, A. M. Nakamura, K. Ogawa, S. Sugita, T. Morota, R. Honda, S. Kameda, E. Tatsumi, Y. Cho, K. Yoshioka, Y. Yokota, M. Hayakawa, M. Matsuoka, N. Sakatani, M. Yamada, T. Kouyama, H. Suzuki, C. Honda, T. Yoshimitsu, T. Kubota, H. Demura, T. Yada, M. Nishimura, K. Yogata, A. Nakato, M. Yoshitake, A. I. Suzuki, S. Furuya, K. Hatakeda, A. Miyazaki, K. Kumagai, T. Okada, M. Abe, T. Usui, T. R. Ireland, M. Fujimoto, T. Yamada, M. Arakawa, A. Fujii, S. Hasegawa, N. Hirata, N. Hirata, C. Hirose, S. Hosoda, Y. Iijima, H. Ikeda, M. Ishiguro, Y. Ishihara, T. Iwata, S. Kikuchi, K. Kitazato, D. S. Lauretta, G. Libourel, B. Marty, K. Matsumoto, T. Michikami, Y. Mimasu, A. Miura, O. Mori, N. Namiki, A. N. Nguyen, L. R. Nittler, H. Noda, R. Noguchi, N. Ogawa, G. Ono, M. Ozaki, H. Senshu, T. Shimada, Y. Shimaki, K. Shirai, S. Soldini, T. Takahashi, Y. Takei, H. Takeuchi, R. Tsukizaki, K. Wada, Y. Yamamoto, K. Yoshikawa, K. Yumoto, M. E. Zolensky, S. Nakazawa, F. Terui, S. Tanaka, T. Saiki, M. Yoshikawa, S. Watanabe, Y. Tsuda, Pebbles and sand on asteroid (162173) Ryugu: In situ observation and particles returned to Earth. *Science (1979)*. **1016**, 1011–1016 (2022).
31. T. Yokoyama, K. Nagashima, Iz. Nakai, E. Young, Y. Abe, Samples returned from the asteroid Ryugu are similar to Ivuna-type carbonaceous meteorites. *Science (1979)*. **33**, 1–12 (2022).
32. J. C. Aponte, J. P. Dworkin, D. P. Glavin, J. E. Elsila, E. T. Parker, H. L. McLain, H. Naraoka, R. Okazaki, Y. Takano, S. Tachibana, G. Dong, S. S. Zeichner, J. M. Eiler, H. Yurimoto, T. Nakamura, H. Yabuta, F. Terui, T. Noguchi, K. Sakamoto, T. Yada, M. Nishimura, A. Nakato, A. Miyazaki, K. Yogata, M. Abe, T. Okada, T. Usui, M. Yoshikawa, T. Saiki, S. Tanaka, S. Nakazawa, Y. Tsuda, S. Watanabe, PAHs,

hydrocarbons, and dimethylsulfides in Asteroid Ryugu samples A0106 and C0107 and the Orgueil (CI1) meteorite. *Earth, Planets and Space*. **75**, 28 (2023).

33. S. S. Zeichner, E. B. Wilkes, A. E. Hofmann, L. Chimiak, A. L. Sessions, A. Makarov, J. M. Eiler, Methods and limitations of stable isotope measurements via direct elution of chromatographic peaks using gas chromotography-Orbitrap mass spectrometry. *Int J Mass Spectrom*. **477**, 116848 (2022).
34. I. Gilmour, C. T. Pillinger, Isotopic compositions of individual polycyclic aromatic hydrocarbons from the Murchison meteorite. *Mon. Not. R. Astron. Soc.* **269**, 235–250 (1994).
35. M. Clog, M. Lawson, B. Peterson, A. A. Ferreira, E. V. Santos Neto, J. M. Eiler, A reconnaissance study of 13C–13C clumping in ethane from natural gas. *Geochim Cosmochim Acta*. **223**, 229–244 (2018).
36. V. V. Kislov, A. I. Sadovnikov, A. M. Mebel, Formation mechanism of polycyclic aromatic hydrocarbons beyond the second aromatic ring. *Journal of Physical Chemistry A*. **117**, 4794–4816 (2013).
37. C. He, R. I. Kaiser, W. Lu, M. Ahmed, Y. Reyes, S. F. Wnuk, A. M. Mebel, Exotic Reaction Dynamics in the Gas-Phase Preparation of Anthracene (C14H10) via Spiroaromatic Radical Transients in the Indenyl-Cyclopentadienyl Radical-Radical Reaction. *J Am Chem Soc*. **145**, 3084–3091 (2023).
38. M. Busso, R. Gallino, G. J. Wasserburg, "Nucleosynthesis in Asymptotic Giant Branch Stars: Relevance for Galactic Enrichment and Solar System Formation" (1999).
39. H. Yabuta, G. D. Cody, C. Engrand, Y. Kebukawa, B. De Gregorio, L. Bonal, L. Remusat, R. Stroud, E. Quirico, L. Nittler, M. Hashiguchi, M. Komatsu, T. Okumura, J. Mathurin, E. Dartois, J. Duprat, Y. Takahashi, Y. Takeichi, D. Kilcoyne, S. Yamashita, A. Dazzi, A. Deniset-Besseau, S. Sandford, Z. Martins, Y. Tamenori, T. Ohigashi, H. Suga, D. Wakabayashi, M. Verdier-Paoletti, S. Mostefaoui, G. Montagnac, J. Barosch, K. Kamide, M. Shigenaka, L. Bejach, M. Matsumoto, Y. Enokido, T. Noguchi, H. Yurimoto, T. Nakamura, R. Okazaki, H. Naraoka, K. Sakamoto, H. C. Connolly, D. S. Lauretta, M. Abe, T. Okada, T. Yada, M. Nishimura, K. Yogata, A. Nakato, M. Yoshitake, A. Iwamae, S. Furuya, K. Hatakeda, A. Miyazaki, H. Soejima, Y. Hitomi, K. Kumagai, T. Usui, T. Hayashi, D. Yamamoto, R. Fukai, S. Sugita, K. Kitazato, N. Hirata, R. Honda, T. Morota, E. Tatsumi, N. Sakatani, N. Namiki, K. Matsumoto, R. Noguchi, K. Wada, H. Senshu, K. Ogawa, Y. Yokota, Y. Ishihara, Y. Shimaki, M. Yamada, C. Honda, T. Michikami, M. Matsuoka, N. Hirata, M. Arakawa, C. Okamoto, M. Ishiguro, R. Jaumann, J.-P. Bibring, M. Grott, S. Schröder, K. Otto, C. Pilorget, N. Schmitz, J. Biele, T.-M. Ho, A. Moussi-Soffys, A. Miura, H. Noda, T. Yamada, K. Yoshihara, K. Kawahara, H. Ikeda, Y. Yamamoto, K. Shirai, S. Kikuchi, N. Ogawa, H. Takeuchi, G. Ono, Y. Mimasu, K. Yoshikawa, Y. Takei, A. Fujii, Y. Iijima, S. Nakazawa, S. Hosoda, T. Iwata, M. Hayakawa, H. Sawada, H. Yano, R. Tsukizaki, M. Ozaki, F. Terui, S. Tanaka, M. Fujimoto, M. Yoshikawa, T. Saiki, S. Tachibana, S. Watanabe, Y. Tsuda, Macromolecular organic matter in samples of the asteroid (162173) Ryugu. *Science (1979)*. **379** (2023), doi:10.1126/science.abn9057.
40. V. Vinogradoff, C. Le Guillou, S. Bernard, L. Binet, P. Cartigny, A. J. Brearley, L. Remusat, Paris vs. Murchison: Impact of hydrothermal alteration on organic matter in CM chondrites. *Geochim Cosmochim Acta*. **212**, 234–252 (2017).

41. T. M. McCollom, B. S. Lollar, G. Lacrampe-Couloume, J. S. Seewald, The influence of carbon source on abiotic organic synthesis and carbon isotope fractionation under hydrothermal conditions. *Geochim Cosmochim Acta*. **74**, 2717–2740 (2010).
42. R. Alexander, R. I. Kagi, A. V. Larcher, Clay catalysis of aromatic hydrogen-exchange reactions. *Geochim Cosmochim Acta*. **46**, 219–222 (1982).
43. C. M. O. D. Alexander, R. Bowden, M. L. Fogel, K. T. Howard, C. D. K. Herd, L. R. Nittler, The provenances of asteroids, and their contributions to the volatile inventories of the terrestrial planets. *Science (1979)*. **337**, 721–723 (2012).
44. C. le Guillou, S. Bernard, A. J. Brearley, L. Remusat, Evolution of organic matter in Orgueil, Murchison and Renazzo during parent body aqueous alteration: In situ investigations. *Geochim Cosmochim Acta*. **131**, 368–392 (2014).
45. C. M. O. D. Alexander, R. Bowden, M. L. Fogel, K. T. Howard, Carbonate abundances and isotopic compositions in chondrites. *Meteorit Planet Sci*. **50**, 810–833 (2015).
46. W.-K. Wong, E. F. Westrum, "Thermodynamics of polynuclear aromatic molecules I. Heat capacities and enthalpies of fusion of pyrene, fluoranthene, and triphenylenet" (1971).
47. N. Thiagarajan, H. Xie, C. Ponton, N. Kitchen, B. Peterson, M. Lawson, M. Formolo, Y. Xiao, J. Eiler, Isotopic evidence for quasi-equilibrium chemistry in thermally mature natural gases. *Proc Natl Acad Sci U S A*. **117**, 3989–3995 (2020).
48. M. A. Sephton, J. S. Watson, W. Meredith, G. D. Love, I. Gilmour, C. E. Snape, Multiple Cosmic Sources for Meteorite Macromolecules? *Astrobiology*. **15**, 779–786 (2015).
49. S. Zeichner, szeichner/RyuguPAHs. *Zenodo* (2022), , doi:10.5281/zenodo.7434958.
50. A. T. Karp, A. I. Holman, P. Hopper, K. Grice, K. H. Freeman, Fire distinguishers: Refined interpretations of polycyclic aromatic hydrocarbons for paleo-applications. *Geochim Cosmochim Acta*. **289**, 93–113 (2020).
51. T. Yada, M. Abe, T. Okada, A. Nakato, K. Yogata, A. Miyazaki, K. Hatakeda, K. Kumagai, M. Nishimura, Y. Hitomi, H. Soejima, M. Yoshitake, A. Iwamae, S. Furuya, M. Uesugi, Y. Karouji, T. Usui, T. Hayashi, D. Yamamoto, R. Fukai, S. Sugita, Y. Cho, K. Yumoto, Y. Yabe, J. Bibring, C. Pilorget, V. Hamm, R. Brunetto, L. Riu, L. Lourit, D. Loizeau, G. Lequertier, A. Moussi-soffys, S. Tachibana, H. Sawada, R. Okazaki, Y. Takano, K. Sakamoto, Y. N. Miura, H. Yano, T. R. Ireland, T. Yamada, M. Fujimoto, K. Kitazato, N. Namiki, N. Hirata, Y. Ishihara, K. Matsumoto, H. Noda, R. Noguchi, Preliminary analysis of the Hayabusa2 samples returned from C-type asteroid Ryugu. *Nat Astron*. **6**, 214–220 (2022).
52. C. D. Vitzthum von Eckstaedt, K. Grice, M. Ioppolo-Armanios, D. Kelly, M. Gibberd, Compound specific carbon and hydrogen stable isotope analyses of volatile organic compounds in various emissions of combustion processes. *Chemosphere*. **89**, 1407–1413 (2012).
53. S. L. Lyons, A. T. Karp, T. J. Bralower, K. Grice, B. Schaefer, S. P. S. Gulick, J. v. Morgan, K. H. Freeman, Organic matter from the Chicxulub crater exacerbated the K-Pg impact winter. *Proc Natl Acad Sci U S A*. **117**, 25327–25334 (2020).
54. J. Eiler, J. Cesar, L. Chimiak, B. Dallass, K. Grice, J. Griep-Raming, D. Juchelka, N. Kitchen, M. K. Lloyd, A. Makarov, R. Robins, J. Schwieters, Analysis of molecular isotopic structures at high precision and accuracy. *Int J Mass Spectrom*. **422**, 126–142 (2017).

55. A. Makarov, Electrostatic Axially Harmonic Orbital Trapping : A High-Performance Technique of Mass Analysis. *Anal Chem* (2000).
56. A. E. Hofmann, L. Chimiak, B. Dallas, J. Griep-Raming, D. Juchelka, A. Makarov, J. Schwieters, J. M. Eiler, Using Orbitrap mass spectrometry to assess the isotopic compositions of individual compounds in mixtures. *Int J Mass Spectrom.* **457**, 116410 (2020).
57. K. Slavicinska, D. Duca, D. Egorov, T. Mitra, Y. Carpentier, C. Focsa, C. J. Bennett, C. Pirim, Link between Polycyclic Aromatic Hydrocarbon Size and Aqueous Alteration in Carbonaceous Chondrites Revealed by Laser Mass Spectrometry. *Earth and Space Chemistry* (2022), doi:10.1021/acsearthspacechem.2c00022.
58. B. P. Basile, B. S. Middleditch, J. Or, Polycyclic aromatic hydrocarbons in the Murchison meteorite. *Org Geochem*. **5**, 211–216 (1984).
59. K. Pering, C. Ponnamperuma, Aromatic Hydrocarbons in the Murchison Meteorite. *Science (1979)*. **173**, 237–240 (1971).
60. M. R. Wing, J. L. Bada, Geochromatography on the parent body of the carbonaceous chondrite Ivuna. *Geochim Cosmochim Acta*. **55**, 2937–2942 (1991).
61. D. W. Sears, Temperature gradients in meteorites produced by heating during atmospheric passage. *Modern Geology*. **5** (1975).
62. C. N. Shingledecker, Thermally induced chemistry of meteoritic complex organic molecules: a new heat-diffusion model for the atmospheric entry of meteorites. *Astrobiology* (2014).
63. C. Mehta, A. Perez, G. Thompson, M. A. Pasek, Caveats to exogenous organic delivery from ablation, dilution, and thermal degradation. *Life*. **8** (2018), doi:10.3390/life8020013.
64. H. Naraoka, A. Shimoyama, K. Harada, Isotopic evidence from an Antarctic carbonaceous chondrite for two reaction pathways of extraterrestrial PAH formation. *Earth Planet Sci Lett*. **184**, 1–7 (2000).
65. Y. Huang, J. C. Aponte, J. Zhao, R. Tarozo, C. Hallmann, Hydrogen and carbon isotopic ratios of polycyclic aromatic compounds in two CM2 carbonaceous chondrites and implications for prebiotic organic synthesis. *Earth Planet Sci Lett*. **426**, 101–108 (2015).
66. M. A. Sephton, C. T. Pillinger, I. Gilmour, δ13C of free and macromolecular aromatic structures in the Murchison meteorite. *Geochim Cosmochim Acta*. **62**, 1821–1828 (1998).
67. M. A. Sephton, I. Gilmour, Aromatic Moieties in Meteorites: Relics of Interstellar Grain Processes? *Astrophys J*. **540**, 588–591 (2000).
68. H. Naraoka, H. Mita, M. Komiya, A. Shimoyama, dD of individual PAHs from the Murchison and an Antarctic carbonaceous chondrite. *Geochim. Cosmochim. Acta, Spec. Suppl. A.* **5** (2002).
69. S. Zeichner, caltechorbi/OrbitrapDataProcessing: orbicodeV1.0.3 (2021), , doi:10.22002/D1.2170.
70. RStudio, RStudio: Integrated Development for R. *RStudio, Inc., Boston, MA* (2020), p. http://www.rstudio.com/.
71. S. M. Messenger, S. A. Mari, X. G. Ao, R. M. W. Alker, Indigenous polycyclic aromatic hydrocarbons in circumstellar graphite grains from primitive meteorites. *Astrophys J*. **502**, 284–295 (1998).
72. T. Maruoka, C. Koeberl, J. I. Matsuda, Y. Syono, Carbon isotope fractionation between graphite and diamond during shock experiments. *Meteorit Planet Sci*. **38**, 1255–1262 (2003).

73. Urey, The Thermodynamic Properties of Isotopic Substances. *Liverbridge Lecture, Chemical Society* (1947).
74. J. Bigeleisen, M. G. Mayer, Calculation of equilibrium constants for isotopic exchange reactions. *J Chem Phys*. **15**, 261–267 (1947).
75. A. D. Becke, A new mixing of Hartree–Fock and local density- functional theories. *J Chem Phys*. **98**, 1372–1377 (1993).
76. D. E. Woon, T. H. Dunning, Gaussian basis sets for use in correlated molecular calculations. III. The atoms aluminum through argon. *J Chem Phys*. **98**, 1358–1371 (1993).
77. F. R. Manby, T. F. Miller Iii, P. J. Bygrave, F. Ding, T. Dresselhaus, F. A. Batista-Romero, A. Buccheri, C. Bungey, S. J. R. Lee, R. Meli, K. Miyamoto, C. Steinmann, T. Tsuchiya, M. Welborn, T. Wiles, Z. Williams, "entos: A quantum molecular simulation package," (available at https://www.threadingbuildingblocks.org.).
78. J. R. Rustad, Ab initio calculation of the carbon isotope signatures of amino acids. *Org Geochem*. **40**, 720–723 (2009).
79. Y. Zhang, Y. Liu, The theory of equilibrium isotope fractionations for gaseous molecules under super-cold conditions. *Geochim Cosmochim Acta*. **238**, 123–149 (2018).
80. R. D. Bardo, M. Wolfsberg, The nuclear mass dependence of the adiabatic correction to the Born–Oppenheimer approximation. *J Chem Phys*. **62**, 4555–4558 (1975).
81. Z. Wang, E. A. Schauble, J. M. Eiler, Equilibrium thermodynamics of multiply substituted isotopologues of molecular gases. *Geochim Cosmochim Acta*. **68**, 4779–4797 (2004).
82. R. Krishnamurthy, S. Epstein, J. Cronin, S. Pizzarello, G. Yuen, Isotopic and molecular analyses of hydrocarbons and monocarboxylic acids of the Murchison meteorite *. *Geochim Cosmochim Acta*. **56** (1992).
83. M. Studier, R. Hayatsu, E. Anders, Origin of organic matter in early solar system-V. Further studies of meteoritic. *Geochimica et Cosmochimica Act*. **36**, 189–215 (1972).
84. J. H. Hahn, R. Zenobi, J. L. Bada, R. N. Zare, Application of two-step laser mass spectrometry to cosmogeochemistry: Direct analysis of meteorites. *Science (1979)*. **239**, 1523–1525 (1988).
85. O. Botta, Z. Martins, C. Emmenegger, J. P. Dworkin, D. P. Glavini, R. P. Harvey, R. Zenobi, J. L. Bada, P. Ehrenfreund, Polycyclic aromatic hydrocarbons and amino acids in meteorites and ice samples from LaPaz Icefield, Antarctica. *Meteorit Planet Sci*. **43**, 1465–1480 (2008).
86. Z. Martins, P. Modica, B. Zanda, L. L. S. d'Hendecourt, The amino acid and hydrocarbon contents of the paris meteorite: Insights into the most primitive cm chondrite. *Meteorit Planet Sci*. **50**, 926–943 (2015).
87. F. L. Plows, J. E. Elsila, R. N. Zare, P. R. Buseck, Evidence that polycyclic aromatic hydrocarbons in two carbonaceous chondrites predate parent-body formation. *Geochim Cosmochim Acta*. **67**, 1429–1436 (2003).
88. H. Naraoka, A. Shimoyama, M. Komiya, H. Yamamoto, K. Harada, Hydrocarbons in the Yamato-791198 Carbonaceous Chondrite from Antarctica. *Chem Lett*, 831–834 (1988).
89. M. Lecasble, L. Remusat, J.-C. Viennet, B. Laurent, S. Bernard, Polycyclic aromatic hydrocarbons in carbonaceous chondrites can be used as tracers of both pre-accretion and secondary processes. *Geochim Cosmochim Acta*. **335**, 243–255 (2022).

90. H. v. Graham, J. E. Elsila, J. P. Dworkin, S. A. Sandford, J. C. Aponte, Deuterium Isotope Fractionation of Polycyclic Aromatic Hydrocarbons in Meteorites as an Indicator of Interstellar/Protosolar Processing History. *Life*. **12**, 1368 (2022).

Acknowledgments: We thank Geoff Blake, Karin Oberg, Larry Nittler, and Laurent Remusat for enlightening discussions. Nami Kitchen, Alex Sessions, and Fenfang Wu provided invaluable experimental insights. Thanks to Tim Csernica, Elliott Mueller, Gabriella Weiss, Peter Martin, Max Lloyd, Andreas Hilkert, Kostya Ayzikov, and Caj Neubauer for their contributions to the development of data analysis software. The authors thank the project members of the Extraterrestrial Samples Curation Center (ESCuC) and the Astromaterials Science Research Group (ASRG) at Institute of Space and Astronautical Science (ISAS) for the sample processes. A portion of this research was carried out by an employee of the Jet Propulsion Laboratory, under a contract with the National Aeronautics and Space Administration (80NM0018D0004)

Funding:
NSF Graduate Research Fellowship (SSZ; JME).
NASA Emerging Worlds Grant #18-EW18_2-0084; (SSZ; AEH; JME).
Simons Foundation Collaboration on the Origins of Life (SSZ; SB; JME).
DOE BES Grant # DE-SC0016561 (JME)
NASA Consortium for Hayabusa2 Analysis of Organic Solubles (JCA; JPD; DPG; JEE)
This research is partly supported by the Japan Society for the Promotion of Science (JSPS) on the grant numbers (21KK0062, YT; 20H00202, HN; JP20H00202, HN; JP20H05846, HN). The burn experiments were funded by Australian Research Council (ARC) for support of a Discovery Outstanding Research Award #DP130100577 KG) and ARC Laureate fellowship (# FL210100103 KG).

Author contributions:

Conceptualization: SSZ, JCA, JME, HNar, YTak, JPD

Methodology: SSZ, AEH, GDon, JME

Investigation: SSZ, JME, SBha, AEH, GDon, JCA, JPD, DPG, JEE, HNar, YTak, STas, ATK, AIH, KG, KHF, HYur, TNak, TNog, ROka, HYab, KSak, TYad, MNis, ANak, AMiy, KYog, MAbe, TOka, TUsu, MYos, TSai, SatoshiTan, FTer, SNak, SWat, YTsu, KHam, KFuk, DAok, MHas, HMit, YChi, NOhk, NOO, SSak, ETP, HLM, F-RO-D, VVui, RThi, CWol, PSK, ARuf, TKog, JIsa, NHer, YOba, TosYos, DAra, HSug, TKog, AFur, KSas, HSat, YFur, JAok, KKano, SMN, TakYos, SatoruTan, MMor, MOno, FKab, KFuj, TYam, YKim

Visualization: SSZ, SBha

Data analysis: SSZ, AEH, GDon, SBha, JME, HYur, TNak, TNog, ROka, HYab, KSak, TYad, MNis, ANak, AMiy, KYog, MAbe, TOka, TUsu, MYos, TSai, SatoshiTan, FTer, SNak, SWat, YTsu, KHam, KFuk, DAok, MHas, HMit, YChi, NOhk, NOO, SSak, ETP, HLM, F-RO-D, VVui, RThi, CWol, PSK, ARuf, TKog, JIsa, NHer, YOba, TosYos, DAra, HSug, TKog, AFur, KSas, HSat, YFur, JAok, KKano, SMN, TakYos, SatoruTan, MMor, MOno, FKab, KFuj, TYam, YKim

Modeling: SSZ, SBha, JME

Funding acquisition: SSZ, AEH, JME, JPD

Project administration: SSZ, JME, STas, HNar, YTak, JPD, HYur, TNak, TNog, ROka, HYab, KSak, TYad, MNis, ANak, AMiy, KYog, MAbe, TOka, TUsu, MYos, TSai,

SatoshiTan, FTer, SNak, SWat, YTsu, KHam, KFuk, DAok, MHas, HMit, YChi, NOhk, NOO, SSak, ETP, HLM, F-RO-D, VVui, RThi, CWol, PSK, ARuf, TKog, JIsa, NHer, YOba, TosYos, DAra, HSug, TKog, AFur, KSas, HSat, YFur, JAok, KKano, SMN, TakYos, SatoruTan, MMor, MOno, FKab, KFuj, TYam, YKim

Supervision: JME, JPD

Writing – original draft: SSZ, SBha, JME

Writing – review & editing: All authors

Competing interests: The authors declare no conflicts of interest. **Data and materials availability**: All processed data are available in the main text or the supplementary materials (*21*). Raw data are available online in (*49*). We declare that all these database publications are compliant with ISAS data policies (www.isas.jaxa.jp/en/researchers/data-policy/). The Hayabusa2 project is releasing raw data on the properties of the asteroid Ryugu in the Hayabusa2 Science Data Archives (DARTS, https://www.darts.isas.jaxa.jp/planet/project/hayabusa2/).

Supplementary Materials

Materials and Methods
Density functional theory (DFT) model of acetylene equilibrium fractionation
Tables S1 to S3
Figures S1 to S6

Table 1. Abundance and isotope ratio measurements. $\delta^{13}C$, δD and $\Delta 2x^{13}C$ values of PAHs extracted from Ryugu samples A0106 and C0107, and Murchison, alongside constraints from terrestrial standards. n = number of replicate analyses. σ = 1 standard error propagated in quadrature (*21*).

Compound (Standard source and Lot #)	**A0106 abundance** (ppm)	**C0107 abundance** (ppm)	**Terrestrial standard $\delta^{13}C$ value** (*n*, **σ**, VPDB, ‰)	**A0106 $\delta^{13}C$ value** (*n*, **σ**; VPDB, ‰)	**C0107 $\delta^{13}C$ value** (*n*, **σ**; VPDB, ‰)	**Terrestrial standard δD value** (n, **σ** ; VSMOW, ‰)	**C0107 δD value** (*n*, **σ**; VSMOW, ‰)	**Terrestrial standard $2x^{13}C/^{12}C$** (*n*, **σ**)	**C0107 $2x^{13}C/^{12}C$** (*n*, **σ**)	**C0107 Δ_{2x13C} (σ, ‰)**	**Murchison $\delta^{13}C$ value** (*n*, **σ**; VPDB, ‰)	**Murchison Δ_{2x13C} (σ, ‰)**
Naphthalene	0.20	0.06	-23.8 (*2*, **0.5**)	-27.5 (*2*, **24.6**)	-20.3 (*3*, **4.9**)	-67.3 (3, **0.4**)	-7.2 (*4*, **36.0**)	0.0048 (*7*, **0.0060)**	0.0050 (*7*, **0.0107)**	35 (**12**)	-	-
Phenanthrene	0.33	0.04	-24.4 (*2*, **0.6**)	-14.9 (*2*, **6.9**)	-12.6 (*3*, **4.2**)	-115.0 (3, **1.1**)	-458.9 (*4*, **31.0**)	0.0095 (*7*, **0.0046)**	0.0097 (*7*, **0.0066)**	-4 (**8**)	-	-
Anthracene	0.15	0.04	-24.1 (*2*, **0.5**)	-10.5 (*2*, **0.5**)	-16.7 (*3*, **4.5**)	-98.9 (6, **0.3**)	-581.3 (*4*, **41.2**)	0.0095 (*7*, **0.0043)**	0.0097 (*7*, **0.0088**)	3 (**10**)	-	-
Fluoranthene	1.33	0.30	-24.2 (*2*, **0.4**)	-27.1 (*2*, **9.8**)	-17.1 (*3*, **2.5**)	-102.0 (6, **1.2**)	-137.0 (*4*, **18.9**)	0.0122 (*7*, **0.0025)**	0.0125 (*7*, **0.0050**)	9 (**5**)	-9.9 (*3*, **1.0)**	51 (**13**)
Pyrene	6.19	1.13	-25.2 (*2*, **0.5**)	-29.6 (*2*, **1.3**)	-23.6 (*3*, **2.1**)	-66.8 (6, **1.2**)	-68.0 (*4*, **15.3**)	0.0122 (*7*, **0.0023)**	0.0124 (*7*, **0.0039**)	11 (**4**)	-11.3 (*3*, **1.1**)	1 (**13**)

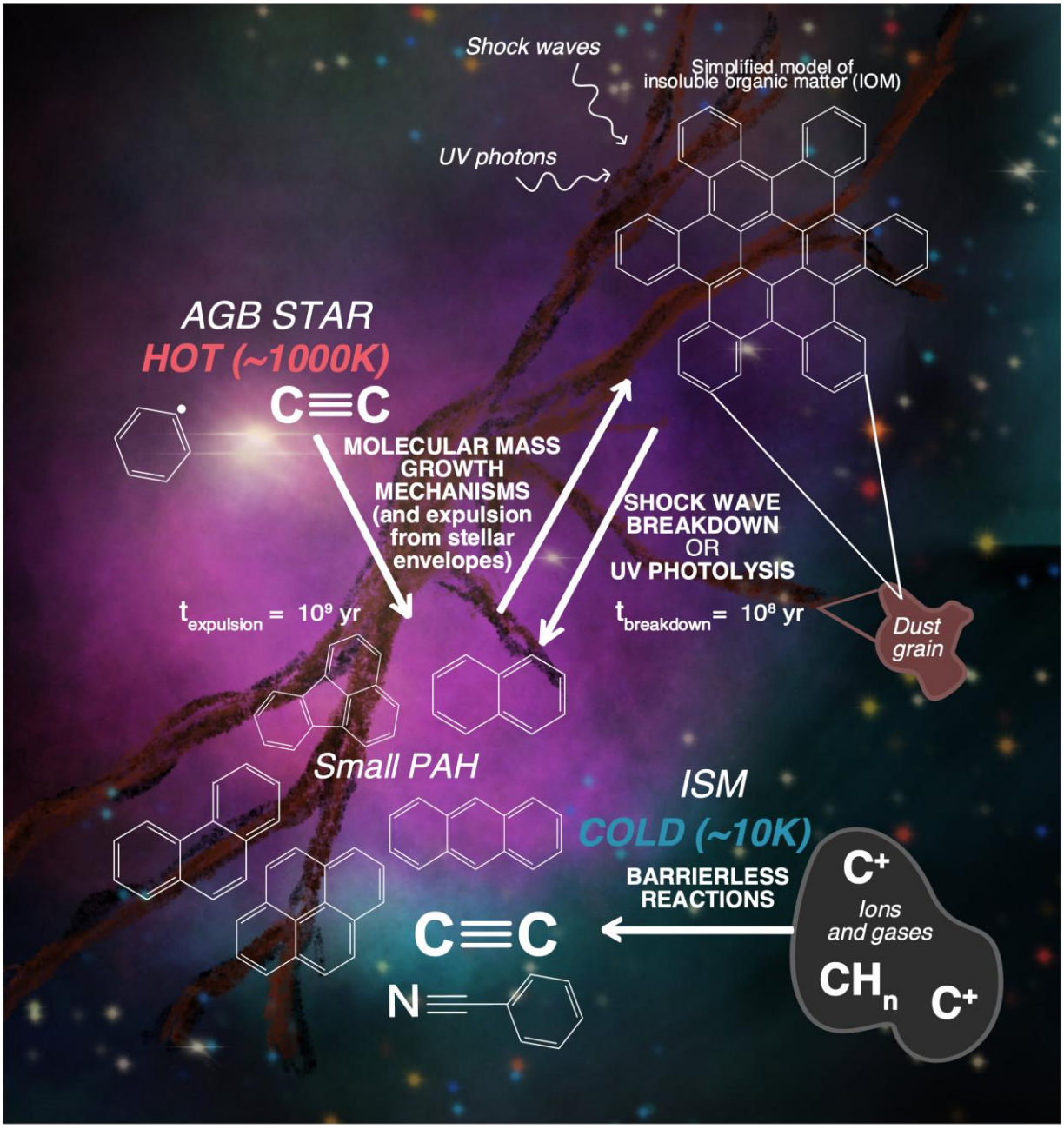

Figure 1. Extraterrestrial PAH formation. PAHs can form in environments ranging from the cold interstellar medium (ISM; ~10-20K) to the hot outflows of carbon-rich stars (~900-1100K). See (*7*) for a comprehensive review of PAH formation processes. Hexabenzocoronene is shown here as a model of the high degree of aromaticity observed in insoluble organic matter (IOM) found within carbonaceous chondrites.

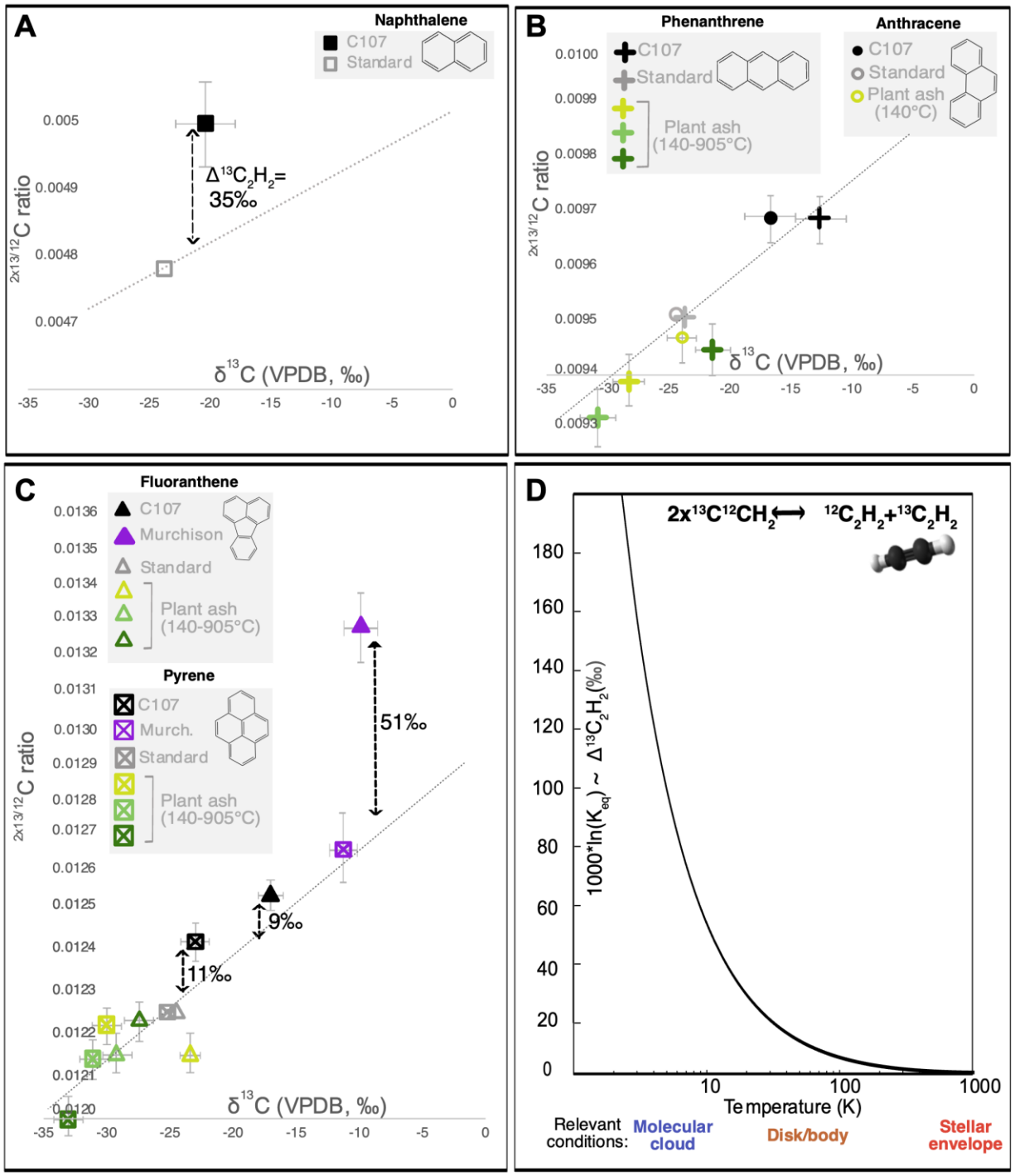

Figure 2. Doubly-^{13}C-substituted compositions. $^{2x13}C/^{12}C$ ratios of (**A**) 2-ring (naphthalene, black square), (**B**) 3-ring (phenanthrene, black cross, and anthracene, black circle), and (**C**) 4-ring (fluoranthene, black triangle, and pyrene, black open crossed square) PAHs from Ryugu sample C0107, Murchison meteorite (purple triangle and open crossed square) and residues of C3 plant biomass (green symbols; (*21*, *50*)), along with the isotope ratios of terrestrial standards (unfilled grey symbols). Stochastic distributions are plotted as dotted grey lines. Departures from stochasticity ($\Delta 2x^{13}C$ values) are represented with labeled vertical arrows. $\Delta 2x^{13}C$ values and

stochastic distributions are calculated and reported as departures from the standard reference frame, i.e., by renormalizing all data such that the standard data conform to a stochastic model for the proportions of isotopologues in the standard.
(**D**) Density-functional and Urey-Bigeleisen-Meyer theory model of the equilibrium fractionation between the singly- and doubly-^{13}C substituted forms of acetylene (*21*). All error bars in panels A-C represent 1σ (Table 1; Table S3).

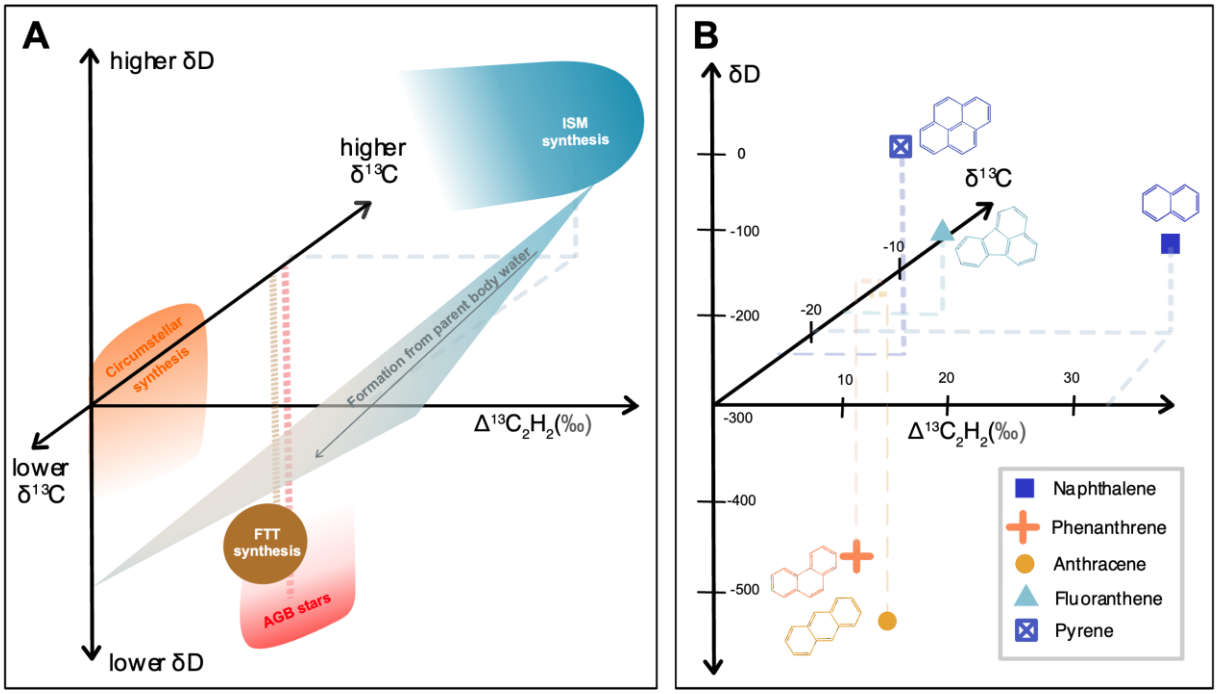

Figure 3. Interstellar PAH formation. (**A**) Distinct processes of synthesizing extraterrestrial PAHs have characteristic δD, $\delta^{13}C$ and $\Delta 2x^{13}C$ values. (**B**) Higher δD and $\Delta 2x^{13}C$ values of naphthalene, pyrene, and fluoranthene from Ryugu suggest 10s-of-percent of these compounds formed via ISM synthesis, while phenanthrene and anthracene are low in δD composition and have approximately stochastic $\Delta 2x^{13}C$ values suggesting synthesis either surrounding AGB stars or via FTT chemistry, potentially influenced by mixing with PAHs formed from parent body aqueous alteration.

Supplemental Materials for

Isotopic evidence of interstellar contributions to formation of polycyclic aromatic hydrocarbons from the Ryugu asteroid

S. Zeichner* et al.

*Corresponding author: S. Zeichner, szeichner@caltech.edu

This PDF file includes:

Materials and Methods

Ryugu sample collection and preparation

The Hayabusa2 mission collected 5.4 total grams of sample from two locations on near-Earth carbonaceous asteroid (1623173) Ryugu and returned them to Earth under carefully controlled conditions (*30*, *51*)). The first sample (Chamber A) was collected 2019 February 21 from the surface and the second (Chamber C) 2019 July 11 from the near-subsurface plume created by the Small Carry-on Impactor. These samples are the most un-weathered examples of carbon-rich extraterrestrial material studied to date (*31*).

Samples were allocated by JAXA for soluble organic analysis, which included a sequential solvent extraction of 17.15 mg A0106, 17.36 mg of C0107, 17.56 mg Orgueil CI-type meteorite, and 16.21 mg of serpentine from hexane to dichloromethane (DCM) to methanol to water (Figure S1A; (*24*)). The serpentine was prepared as a blank alongside the Ryugu samples to ensure no contamination by the compounds of interest was introduced during the preparatory chemistry (Table S1). We note that there was not enough remaining extract from Orgueil following GSFC analyses to analyze that sample using the GC-Orbitrap methods described in this study.

200 µL of each solvent extracted fraction (total of 600 µL) was sent to NASA Goddard Space Flight Center (GSFC) where untargeted GCXGC-ToF-MS and GC-QMS analyses were performed (*32*). These analyses identified endogenous organics within each solvent extract, which were compared with abundances of organics within extracts of Orgueil and serpentine blank (*32*). The residual 5.5 µL and 23.6 µL of the extracts of A0106 and C0107, respectively, were shipped to Caltech in January 2022, where they were stored in a -20°C freezer upon arrival until the time of measurement in April 2022.

Fire product samples and sample preparation

Dry material (a mix of leaves, duff, bark, twigs, and branches) from gingko (*Ginkgo biloba*), cycad (*Cycas spp*) and marri (*Eucalyptus diversi*) were combusted at 142°C, 594°C and 905°C, respectively, within a ventilated tent with an air blower to maintain sufficient O_2 as described in prior studies (*50*, *52*). Volatile organic compounds released from combusted plants are reported in (*52*). Burn residues were collected and stored in glass jars, and then organics were extracted via Soxhlet extraction with a 9:1 azeotrope of dichloromethane (DCM) and methanol (MeOH). The remaining extracts following measurements in (*50*) were fully dried (estimated to have 100-1000s pmol per PAH remaining per vial of sample) and sent to Caltech from Curtin University. Dried vials were stored in the same -20°C freezer as the Hayabusa2 sample extracts upon arrival. Combusted plant samples were resuspended in DCM prior to analysis on the GC-Orbitrap. We used the same batch of DCM across all measurements (combusted plant matter and standards), which we tested prior to addition for presence of any contaminant PAHs that could affect measurements. Plant extracts were measured on the GC-Orbitrap in September 2022, following the same methods described below that were used to analyze the Ryugu sample extracts in April 2022.

Standard sources and preparatory chemistry

Pure standards of naphthalene (Sigma Aldrich 84679-250 mg, Lot #BCCCD4410), phenanthrene (Sigma Aldrich 73338-100mg, Lot# BCCC1654), anthracene (Sigma Aldrich 31581-250mg, Lot#BCCB5640), fluoranthene (Sigma Aldrich 11474-100mg, Lot#BCCD1403)

and pyrene (Sigma Aldrich 18868, Lot#BCCB9571) of known $\delta^{13}C_{VPDB}$ and δD_{VSMOW} values were weighed into 2 mL GC vials (±0.01mg error on standard mass). The molecular average $\delta^{13}C_{VPDB}$ values of the five PAH standards (i.e., one for each sample compound of interest) were characterized by Elemental Analyzer-Isotope Ratio Mass Spectrometry (EA-IRMS) at Caltech. The mean $\delta^{13}C_{VPDB}$ values of naphthalene, phenanthrene, anthracene, fluoranthene and pyrene standards were -23.8±0.5 ‰, -24.4±0.6 ‰, -24.1±0.5‰, -24.2±0.4 ‰, -25.2±0.5 ‰, respectively (Table 1). Likewise, the molecular average δD_{VSMOW} values of the PAH standards were characterized by Temperature Conversion Elemental Analysis (TC/EA) at The University of Wyoming Stable Isotope Facility. The mean δD_{VSMOW} values of naphthalene, phenanthrene, anthracene, fluoranthene and pyrene standards were -67.3±0.4 ‰, -115.0±1.1 ‰, -98.9±0.3 ‰, -102.0±1.2 ‰, -66.8±1.2 ‰, respectively (Table 1). 1 mL of dichloromethane (DCM; Honeywell GC 299-4 EB279-US) was added to each of the vials, which were then sonicated at room temperature for 10 minutes to ensure full dissolution of the PAH. Each PAH standard solution was serially diluted and gravimetrically mixed with each other to form solutions of known molarities of the 5 PAHs of interest. To ensure complete mixing and homogenous concentration of the PAH standard within each vial, we pumped the solvent with a syringe ten times (10x) each before pulling up any standard-solvent mixture for dilution or mixing.

Prior to analysis, we vortexed each sample for 20 seconds to re-suspend any compounds stuck to the walls in solution. Following an injection of A0106, PAH standards of known molarities were mixed together, in proportions scaled to match the concentrations present in the sample extract. Initial concentrations of PAHs in the standard mixture were based on the mass spectral peak height of a standard of known composition and how that compared to the observed peak height of the initial injection of A0106. It took a few times iterating on the amount of each compound added to accurately sample-standard match each PAH, as concentration does not scale linearly with mass spectral peak intensity on the Orbitrap. The relative concentrations of PAHs – the concentration of each of the PAHs in the sample compared to one another – were comparable for A0106 and C0107, and thus the same standard mixture was used for measurements of both samples. A similar process was followed for mixing standards for comparison with the combusted plant biomass samples.

Samples and standards were measured in series under closely matched experimental conditions and amounts of each compound analyzed in experiment. Solvent blanks of DCM were analyzed on the GC-Orbitrap mass spectrometer prior to any standard solution preparation to ensure that there was no PAH background contribution from the solvent. Likewise, a serpentine blank was prepared and run in series with the samples and standards to ensure that it had a concentration of PAHs comparable to the instrumental background (Table S1).

Orbitrap mass spectrometry

Measurements were performed at Caltech on a Thermo Fisher QExactive mass spectrometer with samples introduced via a Trace 1310 GC equipped with a TG-5SilMS chromatographic column (30m long, 0.25 mm ID, 0.25 um film; Fig. S1). Our column choice was based off methods reported by past studies measuring the isotopic compositions of extraterrestrial and terrestrial PAHs via GC-IRMS (e.g., (*32*, *50*, *53*)). The samples and standards were injected via split-splitless injector (275°C) operating in splitless mode. Helium was used as a carrier gas at a constant flow rate of 1.4 mL/min. For our analyses, we used the following oven ramp, which was optimized to separate the target compounds of interest: 50 to 110°C at 2°C/min, 5 minute hold at 110°C, 110 to 145°C by 2°C/min, 10 minute hold at 145°C, 145 to 170°C by

2°C/min, 5 minute hold at 170°C, 170 to 260°C by 2°C/min, 5 minute hold at 260°C, and 260 to 295°C by 20°C/min, followed by a 20 minute hold. This oven ramp was optimized specifically to separate the PAHs of interest from one another, but was adapted from the ramp used by Aponte et al. in the preliminary GSFC characterization of extracted organics from the Ryugu samples (*32*). A similar ramp was used to measure the fire products, however for those measurements we used a faster ramp from 50 to 110 °C (i.e., 20°C/min) to improve the separation between isomers. We did not observe any effect of this ramp on the peak shapes of target PAHs.

We measured PAHs extracted from the Hayabusa2 samples in DCM using the "direct elution method," a recent development in Orbitrap isotope ratio mass spectrometry that introduces the eluent directly from the GC column into the mass spectrometer without intermediate peak trapping (*33*). This method allows characterization of multiple compounds within a complex mixture in a single experiment, which is particularly useful in this experiment because it reduces the amount of sample size needed compared to those required for peak-trapping methods that capture and focus on a single compound in a chromatogram (Figure S1&2; (*33*)). The direct elution method also improves chromatographic peak shapes and compound separation by bypassing valves and plumbing within our GC system (*54*) by connecting the GC column directly to the Orbitrap transfer line via a Valco union.

For the Hayabusa2 samples considered here, where the currently available samples are small and concentrations of organics are low (picomole to sub-picomole of each PAH of interest per 1 μL of sample), the direct elution method is capable of achieving measurements of isotopic properties of interest with per-mille-level precision, which is sufficient for our purposes of characterizing the large isotopic contrasts between terrestrial and many forms of extraterrestrial organics, and differences in multiply-substituted chemical isotope effects between high and very low temperature conditions.

Orbitraps can perform measurements at high resolutions required to separate ^{13}C and D isotopologues simultaneously (*33*); thus a single measurement can provide useful information to constrain several isotopic properties (i.e., $\delta^{13}C$, δD and $^{2x13}C/^{12}C$). Moreover, naphthalene, phenanthrene, anthracene, fluoranthene and pyrene are all relatively stable aromatic compounds that do not readily fragment when introduced into the EI ion source (Figure S2). Therefore, their mass spectra on the GC-Orbitrap are dominated by the molecular ions, including the singly- and doubly-substituted isotopologues of the molecular ions, which makes them excellent candidates for measurement via the direct elution method (*33*).

The direct elution measurements were performed via GC-Orbitrap as follows: GC effluent was transferred directly into the ion source via a heated transfer line (260°C) where analytes were ionized via electron impact (EI; Thermo Scientific Extractabrite, 70eV; Fig. 1A, B). Each compound generated a characteristic mass spectra upon ionization (Fig. S2). The ions were extracted from the source, subjected to collisional cooling during transfer through the bent flatpole, underwent mass-window selection by the Advanced Quadrupole Selector™ (AQS), and were then passed through the automatic gain control (AGC) gate prior to storage in the C-trap — a potential-energy well generated by radio frequency and direct current potentials (Fig. S1). Ions accumulated in the C-trap until the total charge reached a user-defined threshold (the "AGC target"), then were introduced into the Orbitrap mass analyzer as a discrete packet. Within the mass analyzer, ions orbit between a central spindle-shaped electrode and two enclosing outer bell shaped electrodes, moving harmonically at frequencies proportional to *m/z* (*55*). The raw data product of this oscillation—the "transient"—is converted via fast Fourier transform into a data product that can be processed for isotope ratio analysis (see *Data processing*).

We refer to each injection of a sample or standard as an "acquisition;" each acquisition is comprised of "scans," and each scan is comprised of ion intensities and m/z ratios averaged by the Orbitrap over a short time interval (200 ms for 120k resolution, with longer-length scans for higher user-defined resolutions). It is critical that every acquisition used for isotope ratio analysis operates under "AGC control," i.e., under conditions where the Automatic Gain Control (AGC) limits the number of ions into the Orbitrap in each scan and this number stays relatively constant from one scan to another. The AGC target is computed as the total ion current times the injection time (TIC*IT) over the course of a single acquisition. Ideally, the TIC*IT value does not vary much from scan to scan.

AGC stability was particularly important for this study, as sample amount was limited and abundances of each PAH within each sample were low. It was clear when the instrument was not performing measurements under AGC control because the IT would reach the user-defined maximum threshold (3000 ms); in these cases, we either increased the amount of sample introduced for the experiment or adjusted experimental parameters, described further below.

Pure PAH standard mixtures were used for method development. Measurements of the standards had several goals: identify the elution time frame of the compounds of interest, identify the characteristic mass spectra for each PAH, optimize the oven ramp to ensure baseline separation of near co-eluting compounds, and perform sensitivity tests to determine how many ions were observed under certain experimental conditions for a known PAH concentration (i.e., 25, 5, 1, and 0.1pmol per 1 µL of solvent, calculated based on the molarity of the first standard solution).

After the oven ramp was optimized, we performed experiments using standard mixtures as follows: a standard solution of the 5 PAHs, each present in concentrations of 5pmol per 1 µL, was injected. We were able to anticipate approximate concentrations of PAHs in the Ryugu DCM extracts based on results published in (*32*), and prepared standard mixtures accordingly. Once we had optimized the method using these standard mixtures, we compared the mass spectral peak intensities of each PAH within this standard to the mass spectral intensities of the 5 PAH peaks in one direct injection of A0106; our first injection was 2 µL of the sample, without any mass jumps or differences in AGC target or resolution for each compound. We used this first injection to calculate the absolute and relative amounts of each PAH in the sample, and then mixed relative concentrations of PAH standards together that were scaled appropriately with the absolute and relative concentrations of PAHs within the sample. Following direct injection of the newly mixed standard scaled to the concentrations of PAHs in A0106, we adjusted the amounts as necessary until the relative abundances matched those measured in A0106 (within a factor of 1.5x). This scaled standard mixture was used as a comparative standard for all subsequent injections and analyses of the Ryugu samples, which were measured in series and with care to ensure close sample-standard matching of concentration and experimental conditions. The relative abundances of PAHs in extracts of A0106 and C0107 were the same (although the absolute abundances in extracts of C0107 were about half those in A0106), so the same standard mixture was used as a reference for measurements of both samples.

Our first sample injection (2 µL of A0106) was done using an 8Da wide mass window (Fig. S2A), $2*10^5$ AGC target, and 120k resolution for compound identification and quantification of concentration relative to measured standards, as described above in "Standard sources and preparatory chemistry." The initial injection was also very important for identifying any potential co-eluents within the mass window of interest for the compounds, as co-eluents that produce mass spectral fragments within the mass window of interest can have detrimental

effects on the accurate measurement of isotope ratios (*56*). The chromatographic peaks of the PAHs in the sample (PAH concentrations were 0.05-1pmol per 2.5μL injection, corresponding to mass spectral peak intensities ("NL scores") of $2*10^4$ to $1*10^6$, a reflection of the great chemical complexity of the organic extracts from the Hayabusa2 samples; (*32*)) were a small fraction of the total ion current for other co-eluting species in the mass spectrometric mass window 50-250 Da.

To address the number of co-eluting compounds, we devised a method whereby we defined several narrower mass windows (either 8 or 2 Da wide; see below), each centered on the expected mass of the ions of interest for one of the PAHs of interest, and the performed 'jumps,' changing the mass range of the quadrupole MS used for ion pre-selection in sync with the elution time of each compound; time periods of elution were constrained by observation of the mixture of PAH standards prior to analysis of the samples. We observed that the jump method technique enabled us to improve the shot noise limit (Eqn. S4) on the measurement of the isotopic composition of our standards by a factor of 2. The chosen PAHs were particularly good candidates for this method, as the two 3- and 4-ring PAHs are isomers of one another, so they elute close together in time and have un-substituted (and substituted) molecular ions of the same mass, allowing one mass window jump to be suitable for observing both compounds. This close elution of the isomers made full baseline separation of the near-co-eluting PAHs of critical importance.

Abundance measurements

We determined the abundance of each PAH within each sample by comparing the measured intensity of the height of the base peak of the molecular ion for that species with the height of the same peak measured for analysis of a standard of known amount. This calibration assumes a linear relationship between sample size and peak intensity and a negligible background for the peaks used for this purpose. These simplifying assumptions were justified by the close matching of concentrations of each compound in samples and standards, and by the negligibly small sizes of relevant peaks in procedural blanks run with pure DCM solvent (Table 1; Table S1).

We report abundances of the same order as abundances reported by Aponte et al. for the same compounds in extracts of both Ryugu and Orgueil samples (Fig. S3A; (*24*, *32*)). Ryugu and Orgueil PAH abundances were one to two orders of magnitude lower than those reported for Murchison and other CM2 chondrites (Fig. S3A). We normalized abundances PAHs from Hayabusa2 to pyrene, and these ratios are comparable to those in other CCs, though on the lower end of the range for naphthalene, phenanthrene and anthracene (Fig. S3B). Pyrene is generally the most abundant PAH within extraterrestrial samples. We were interested in investigating whether relative abundances of distinct PAHs could be linked to any specific characterized properties of the samples. We did not observe any such relationships, though it would be interesting to consider in a future study measuring additional isotopic properties of PAHs from different carbonaceous chondrite samples.

PAHs abundances and distribution patterns vary among different petrologic types, meteorite samples of the same type, and different specimens of the same meteorite (Fig. S3B; *57*). These differences are not traceable to different extraction procedures (e.g., *58*, *59*). Differences in abundance most likely reflects sample heterogeneity and not distinguishing differences among meteorite classes, parent bodies or other larger-scale groupings, but could also reflect analysis by different techniques (i.e., GC-MS versus GC-Orbitrap, etc.). Thus, the

differences in absolute and relative abundances of PAHs between the Hayabusa2 samples and those found in CC's potentially reflect differences that arise from removal or redistribution of PAHs over small spatial scales. These possibly were controlled by PAH volatility and solubility during hydrothermal aqueous alteration on the parent body (*24*), geo-chromatographic separation (*57*, *60*), or, in the case of meteorite samples, organic synthesis or decomposition of PAHs during passage through the Earth's atmosphere (*61–63*).

There were differences in both absolute and relative abundance between PAHs between our study and Aponte et al's. In particular, the concentration of naphthalene was much lower in our samples which may be related to volatilization of naphthalene between the measurements at GSFC and Caltech. During analyses at Caltech, we attempted to mitigate solvent loss as much as possible by immediately recapping the vial each time it was punctured by the syringe for analysis.

Additional uncertainties in our calculation of the PAH abundances could arise from each step of standard preparation and quantification. The initial volume present in the vial was estimated by the number of replicates possible with the given volume before there was no solvent left in the vial; however, we acknowledge that some small amount of solvent may have volatilized (but is difficult to quantify to include in this error estimation). We estimated the error on the microbalance weighing of standards to be 0.15 μg for each 1000 μg of standard weighed out. Each dilution had quantification errors of about 5% relative, which was determined by replicating the dilution of the same solution and observing the intensity of that diluted standard on the GC-Orbitrap. We propagated this error by 3x as each standard solution was diluted three times to arrive at the concentrations present within the standard mixture scaled to the absolute and relative concentrations of A0106. Finally, the variation in the intensity of the mass spectral peaks on the Orbitrap varied by ~20% relative for replicate injections (which incorporated both variation in the injection volume itself, heterogeneity in the concentration of the compound within the final standard mixture, and instrument variation). These three sources of error propagated together generated a combined 25% relative error on the concentration calculations of each PAH, which accounts for most of the differences between our reported values and those of Aponte et al. Concentrations reported by Aponte et al. were also computed gravimetrically, although the estimated error on each measurement is unknown.

Isotope ratio measurements

Acquisitions measured with 8 Da mass windows (2.5 μL solvent injections) for each compound were used for $\delta^{13}C$ measurements (i.e., ratios of singly substituted to unsubstituted isotopologues) and abundance calculations (Fig. S2B). Acquisitions with 2 Da mass windows (4.5 μL solvent injections) were used for measuring the ratios of the D and $2x^{13}C$-substituted mass spectral peaks to the ^{13}C-substituted mass spectral peak (Fig. S2C). The 8 Da mass window measurement were used to convert these ratios into the base peak (unsubstituted mass spectral fragment) reference frame. The combination of these two measurements were used to calculate ratios of D/H and $2x^{13}C/^{12}C$, as explained below). We took care to ensure that all isotope ratio measurements were performed under conditions where the intensities of contaminant peaks totaled to less than 20% of the intensity of the base peak of the target PAH (Fig. S2B&C), a threshold that has been demonstrated to be effective for performing accurate isotope ratio measurements for compounds that are part of complex mixtures and not perfectly purified by preparatory chromatography (*56*).

For each jump, we also varied the AGC targets and mass resolution for the specific observation windows, based on sensitivity tests using standards with the same mass spectral intensities we observed in a measurement of the sample. To maximize sensitivity, we chose the highest AGC target and the lowest resolution possible for each mass window jump, where the full elution of the chromatographic peak of interest could be observed under AGC control. For instance, for the 8Da window measurement of the lower abundance compounds (naphthalene, phenanthrene and anthracene), we used a lower AGC target ($2*10^4$) to ensure that we were able to perform the measurement of the lower abundance compound under AGC control, whereas we used a $1*10^5$ AGC target for the fluoranthene and pyrene window because those compounds were more abundant within the sample. Likewise, we performed all of the 2 Da mass window measurements of the C0107 sample with an AGC target of $2*10^4$ and a resolution of 180k to ensure full separation of the ^{13}C and D mass spectral peaks. Fire product measurements with 8Da mass windows were performed with $1*10^5$ AGC target and 120k resolution. Smaller mass window measurements of fire products were performed with mass windows of 2Da, $2*10^4$ AGC target and with resolutions of 120k. We note that the 120k resolution setting for combusted plant samples was not high enough to measure the δD values of those PAHs. The complete list of experiments, with their experimental parameters are included in the full data table compilation (Table S2).

Molecular-averaged carbon isotope values ($\delta^{13}C_{VPDB}\pm1\sigma$[1]) for naphthalene, phenanthrene, anthracene, fluoranthene and pyrene from A0106 were -27.5±24.6‰, -14.9±6.9‰, -10.5±0.5‰, -27.1±9.8‰, and -29.6±1.3‰, respectively (Table 1; Fig. S4A). Carbon isotope values ($\delta^{13}C_{VPDB}\pm1\sigma$) for naphthalene, phenanthrene, anthracene, fluoranthene and pyrene from C0107 were -20.3±4.9‰, -12.6±4.2‰, -16.7±4.5‰, -17.1±2.5‰, and -23.6±2.1‰, respectively (Table 1; Fig. S4A). We had access to only a small quantity of extract from sample A0106 and were neither able to replicate measurements to our desired level, nor measure isotopic properties other than molecular-averaged $\delta^{13}C$ values. For this reason, we focus our interpretations on data for sample C0107.

Deuterium isotope values ($\delta D_{VSMOW}\pm1\sigma$) for naphthalene, phenanthrene, anthracene, fluoranthene and pyrene from C0107 were -7.2±36.0‰, -458.9±31.0‰, -581.3±41.2‰, -137.0±18.9‰, and -68.0±15.3‰, respectively (Table 1; Fig. S4B). These values are lower than the measured bulk δD_{VSMOW} values of both A0106 and C0107, which were 252±13‰ and 269±13‰, respectively (*24*).

$\delta^{13}C_{VPDB}$ and δD_{VSMOW} values for Ryugu PAHs fell within the range measured for several meteorite samples (Fig. S4A). For Hayabusa2 samples, fluoranthene is ~10‰ enriched in ^{13}C relative to pyrene, and similar to the difference previously observed in CCs (*34*, *64–68*).

We measured PAHs produced by combustion experiments of C3 plants at known temperatures (140-905°C) using the same methods used for measuring the isotopic compositions of the Ryugu PAHs. Combustion-produced PAHs were measured at ~10pmol abundances per injection. We measured the $\delta^{13}C_{VPDB}$ values for plant-derived PAHs, which agreed with values previously measured by traditional continuous-flow IRMS methods for compound-specific isotope analyses (CSIA), within 2 standard deviations (σ) (Table S3; (*50*)).

[1] Reported σ values represent propagated standard errors (*21*).

Data processing for isotope ratio computation

We adapted the data analysis method outlined in Zeichner et al., 2022 to process the data from our measurements. In short, data from each acquisition are converted to selected-mass chromatograms (intensity versus time for a specific *m/z*), which can then be converted into ion counts and used to compute isotope ratios. These data are extracted and converted using a program called *FT Statistic*, which is a proprietary software produced by Thermo Fisher to process Orbitrap data. This software extracts acquisition statistics from .RAW files such as intensity and peak noise, and converts it into a .csv file. We then process the data using an in-house Python processing script (*69*), which is located on the Caltech data repository and described below. Statistics and plots for our experiments were generated with a combination of Excel and RStudio (*70*). Raw data and excel spreadsheets of processed data are available online (*49*).

Prior to any analysis using the Python script, we manually observed the files output by FT Statistic to choose time frames of elution for each of the chromatographic peaks. These time frames were consistent for each PAH and across acquisitions. In some cases, variations in the mass spectral peak intensities of each PAH led to different lengths of time that the compound was observed under AGC control; we chose a consistent and conservative time frame (i.e., the shortest window encompassing the time frame under AGC control for a given PAH across all replicate sample/standard acquisitions) as the period over which to integrate each peak for isotope analysis.

The Fourier transform of the transient data reports signal intensities (NL scores), which can be converted into ion counts as follows:

$$N_{io} = \frac{S}{N} * \frac{C_N}{z} * \sqrt{\frac{R_N}{R}} * \sqrt{\mu}\ (Eqn. S1),$$

where N_{io} is the number of observed ions, S is the reported signal intensity (NL score) for the molecular or fragment ion in question, N is the noise associated with that signal, R is the formal resolution setting (defined for *m/z* 200) used, R_N is a reference formal mass resolution, C_N is the number of charges corresponding to the noise at reference resolution R_N (4.4; a constant established by prior experiments; see Eiler et al., 2017), z is the charge per ion for the fragment of interest, and μ is the number of microscans. We chose scans where the NL score was >5% of the maximum NL score of the chromatographic peak; NL scores from these scans were converted into ions, substituted and base peak ion counts were respectively summed, and then divided to calculate the isotope ratio of interest.

Due to the low abundance of ions observed within each mass window jump, the backgrounds for all compounds for both the 8 Da and 2 Da mass window experiments were never observed under AGC control, which thus made it impossible to apply a quantitative background correction to our isotope measurements. We report the observed intensities of the background versus the maximum intensity of the eluting peak in Table S1; in all cases, the background never exceeded intensities ~10^3. Anthracene had the highest background relative to its peak height (Table S1), which we attribute to the near co-elution with phenanthrene, although we were careful to confirm baseline separate all five PAHs of interest from one another when PAHs standards were injected at concentrations of 5pmol per 1 μL. Future studies that are able to observe the background under AGC control could average the background NL score for the five

scans prior to the elution of the peak timing, and then subtract that NL score from the NL score of the compound of interest prior to conversion to counts, as described in (*33*).

Some of our measurements were performed with imperfect sample-standard intensity matching, or introduced such that the maximum NL scores of compounds varied between acquisitions. As such, because there was variation in the precision of measurements between acquisitions, we chose to weight the acquisitions by the number of ions observed in each acquisition. In particular, we had to apply some additional corrections to the data processing of A0106 singly-^{13}C substituted composition measurements; there was limited sample (5.5 μL) and because it was used for initial sample characterization and to iteratively mix and scale standards appropriately, the two A0106 injections were not measured using the same method and with a direct comparison to a standard with matching concentrations of PAHs. Further adjustments to A0106 data is detailed in *Measurements and standard corrections for acquisitions of A0106*. All data for C0107 measurements were processed as described below. In these cases, we did not apply any drift or scale correction to our data prior to computing error weighted means.

We computed error-weighted means of the sample-standard isotope ratio difference for multiple acquisitions of each compound of interest. We chose to weight each sample and standard isotope ratio by its error so that we could appropriately weight measurements with varied sample and standard intensities that were introduced in the process of sample-standard matching, or observing the same property with different mass window sizes (i.e., $^{2x13}C/^{12}C$ measurements performed with both the 2 Da and 8 Da mass windows). Error weighted means of the measured sample and standard isotope ratios were weighted by the shot noise limit (SNL; approximately equal to standard error (SE) of each acquisition (which is proportional to the number of analyte ions observed for each acquisition) as follows:

$$\hat{\mu} = \frac{\sum_{i=0}^{n} x_i}{{\sigma_i}^2} * \frac{1}{\sum_{i=0}^{n} \frac{1}{{\sigma_i}^2}} \text{ (Eqn. S2)}$$

where x_i is the isotope ratio of each acquisition (n) and σ_i is the SNL of each acquisition. The sample-standard difference was then computed by taking a ratio of the two error-weighted means, which are the values reported in Table 1 and Table S3. Reported sigma values represent 1 standard error (SE, σ), but were also error-weighted as follows:

$$\sigma^2(\hat{\mu}) = \frac{1}{\sum_{i=0}^{n} \frac{1}{\sigma i^2}} \text{ (Eqn. S3).}$$

The shot noise limit (SNL; a proxy of and ~ relative standard error (RSE) of each acquisition, as well as a representation of the number of ions observed of each compound for each acquisition; Eqn S1) was used as the weight for both the calculation of $\hat{\mu}$ and σ($\hat{\mu}$), and was calculated as follows:

$$\frac{\sigma_{SNL}}{R} = \sqrt{\frac{1}{\sum C_{io}} + \frac{1}{\sum c_{io}}} \ (Eqn. S4),$$

where $\frac{\sigma_{SNL}}{R}$ is the shot noise limit on the relative standard error for a single acquisition, which is calculated based on $\sum C_{io}$ and $\sum c_{io,}$ — the sums of all the counts for the substituted and unsubstituted molecular of interest, respectively. Errors reported in sample-standard differences were propagated from the individual errors calculated for sample and standard, respectively, added in quadrature. Isotope ratios for fire product PAHs and associated standard errors were computed without weights, as we had enough sample to perform replicate measurements to equal levels of precision.

Our measured sample-standard difference isotope ratios were converted to international reference frame scales as follows:

$$R_{ref} = \frac{R_{Sample}}{R_{standard}} * R_{(TC)EA} \text{ (Eqn. S5)},$$

where R_{ref} is the isotope ratio of the PAH on the international reference frame scale (i.e., VPDB or VSMOW), R_{Sample} is the measured isotope ratio of PAH from the Ryugu extract or the burned plant biomass, $R_{standard}$ is the isotope ratio of the PAH standard measured under close sample-standard matching conditions, and $R_{(TC)EA}$ is the isotope ratio of the standard on the international reference scale constrained by EA or TC/EA. Isotope ratio measurements performed with 8 Da mass window jumps are already reported relative to the unsubstituted molecular ion reference frame and could be converted directly into the known international reference frame, but isotope ratios performed with 2Da mass windows are measured relative to base peak within that window, i.e., the singly-^{13}C substituted mass spectral peak. To convert 2Da window measurements into the base peak reference frame, we multiplied the sample-standard difference D/^{13}C and ^{2x13}C/^{13}C ratios by the singly-substituted sample-standard difference ^{13}C/^{12}C isotope ratio (already weighted at this point by their respective $\frac{\sigma_{SNL}}{R}$), and then again by the measured isotope ratio of the standard that had been calibrated on the international reference frame scale. As with all our other measurements, errors for each ratio included in computation were added in quadrature; error-weighted sigma values were used for average isotope ratio measurements acquired via GC-Orbitrap measurements, while standard deviations were used for EA and TC/EA measurements. Following conversion to international reference scales, singly-substituted ^{13}C and D isotope ratios were reported in delta notation.

Delta notation presents the isotope ratio measured in a property of a sample relative to the same property measured in a standard of known isotopic composition:

$$\delta = \left(\frac{R_{sample}}{R_{standard}} - 1\right) * 1000 \ (Eqn\ S6),$$

where R values are the error weighted mean isotope ratios of the sample and the standard. R values are often denoted with a superscript to indicate the relevant element and isotopic substitution (i.e., ^{13}R is the ratio of ^{13}C to ^{12}C within a sample). Delta values are reported in units of per-mile (‰). We report singly- ^{13}C and ^{2}H (D) substituted isotopic compositions, as well as doubly-^{13}C substituted isotopic compositions as delta values. All δ^{13}C and δD values have been converted onto the VPDB and VSMOW scales respectively, which are indicated as subscripts.

To compute doubly-substituted ^{13}C isotope ratios for Ryugu sample analyses, we took measurements from both 8 Da and 2 Da mass window acquisitions. We converted 2 Da mass window acquisitions into the unsubstituted mass spectral peak reference frame as described above, and then computed an error weighted mean of the acquisitions from the two different types of measurements. Fire product doubly-substituted ^{13}C isotope ratios were based only on 2Da mass window measurements, converted into the base peak reference frame as described above.

Doubly-^{13}C substituted isotopic compositions are reported in two ways: 1) As raw, measured ^{2x13}C/^{12}C ratios and 2) as Δ^{2x13}C values. Δ^{2x13}C values are reported in units of ‰ and represent the difference between the measured proportion of ^{2x13}C isotopologues in the sample and the proportion it would have had with stochastic distribution of isotopes among all possible isotopologues.

This conversion first calculates the expected ^{2x13}C/^{12}C ratios for the sample and standard based on their respective δ^{13}C values and the assumption that both have a stochastic proportion

of all isotopologues. For example, the stochastic distribution of double-^{13}C-substitutions among isotopologues of pyrene or fluoranthene, which each have 16 carbons, would be equal to:

$$^{13C212C14}R = \frac{[^{13}C]^2[^{12}C]^{14}}{[^{12}C]^{16}} \ (Equation\ S7),$$

where [^{13}C] and [^{12}C] are the fractional abundance of ^{13}C and ^{12}C within a sample with a given ^{13}R value ([^{13}C] = ^{13}R/(1+^{13}R). The same calculations can be performed for naphthalene and phenanthrene/anthracene by assuming a double substitution into a molecular structure with 10 and 14 carbons, respectively.

To compute Δ^{2x13}C values, measured 2x^{13}C/^{12}C ratios were converted into the calculated reference frame, via a conversion factor, α:

$$\alpha = \frac{^{measured}R}{^{true}R} \ (Equation\ S8)$$

where ^{measured}R is the measured 2x^{13}C/^{12}C ratios, and ^{true}R was the calculated value within the expected stochastic reference frame. Once the ratios were converted into this stochastic reference frame, we divided the converted, measured value by the calculated stochastic 2x^{13}C ratio for the sample's measured δ^{13}C value. This quotient was then converted into a Δ^{2x13}C values by subtracting one and multiplying the residual by 1000 to derive a difference in per-mille.

For the purposes of visualizing the data in Figure 2, a similar procedure to above was followed, but all measured isotopologue 2x^{13}C/^{12}C ratios were converted into the measured Hayabusa 2 sample reference frame by scaling measured values by a calculated alpha value (following Equation S8), where the "true value" in this case was the 2x^{13}C/^{12}C ratios as measured during the Hayabusa2 measurement session. Comparing measurements of the isotopic composition of the same standards measured across measurement sessions allowed for easy conversion between the reference frame of one to another.

Importantly, our calculation of Δ^{2x13}C values and our interpretations of their significance depend on the assumption that the standards used for this work have approximately stochastic proportions of isotopologues (and hence error bars are not presented for the standards plotted in Figure 2 as they are stochastic by definition). This simplifying assumption is justified by three arguments: 1) The chemical isotope effects associated with the high temperature reactions used to synthesize commercial PAHs are predicted to lead to negligibly small anomalies of multiply substituted isotopologues (Δ^{2x13}C values within ~1 ‰ of zero). This expectation arises from the well-known dependences of equilibrium and conventional chemical kinetic isotope effects on temperature and the reduced masses of molecular vibrations; 2) measured Δ^{2x13}C anomalies in natural and synthetic ethanes are negligibly small at the levels of precision relevant to this study (*35*), confirming our expectations that chemical isotope effects associated with breaking and forming bonds in hydrocarbons at temperatures of ~300+ K lead to Δ^{2x13}C variations that are small by the standards of the data discussed in this study; and 3) our assumption that our commercial PAH reference standards have stochastic proportions of ^{2x13}C isotopologues leads to the result that the 3-ring PAHs from the Hayabusa2 samples also have stochastic proportions, despite having distinct δ^{13}C values. This result could be fortuitous, but suggests that our reference frame is capable of recognizing differences between samples that are approximately stochastic (phenanthrene and anthracene) and those that depart substantially from a stochastic C

isotope distribution (naphthalene, pyrene and fluoranthene). Our finding that PAHs extracted from burned biomass combusted at 100s of degrees Celsius do not exhibit $\Delta^{2x13}C$ values that deviate significantly from stochastic distribution at the levels of precision within this study help to support our conclusions on the novelty of positive clumped ^{13}C anomalies and their relationship to interstellar synthesis processes (see "*Tests of statistical significance").*

Propagating error to correct for differences in injection volume

In two cases – naphthalene and phenanthrene – we found in replicate measurements of standards of different volumes, the error between the $\Delta 2x^{13}C$ values for 1uL and 5uL injections was larger than 1σ analytical error of replicate measurements of C0107 with a 2Da mass window. In these two cases, we added the error reported for naphthalene and phenanthrene $\Delta 2x^{13}C$ values in Table S5 in quadrature with the experimental error; this is the error reported for those two measurements in Table 1. The error did not change our analyses.

Measurements and standard corrections for acquisitions of A0106

We were not able to measure δD of A0106 PAHs because we did not have enough sample to perform a 2 Da mass window experiment. Likewise, we do not report $^{2x13}C/^{12}C$ ratios because the isotope ratio measurements of the standard bracketing the two acquisitions of the sample did not demonstrate reproducible measurements within the 2*SE acceptable for inclusion. Errors on A0106 measurements of $\delta^{13}C$ values were consistently higher because we were only able to perform two (2) acquisitions with the limited amount of sample, and the first was a direct elution measurement without mass window jump. Each acquisition was performed under distinct conditions (i.e., AGC target, with imperfections in sample-standard concentration matching due to iterating on the creation of the appropriate standard mixture). In particular, differences in the isotope ratio of the naphthalene standard varied for the concentration of naphthalene introduced into the instrument, which we hypothesize may be related to naphthalene being very volatile. Thus, it was necessary in these cases that were performed with fewer replicate acquisitions, larger backgrounds, and without close sample-standard matching to introduce additional corrections to the data processing procedure. For A0106 sample-standard isotope ratio comparison, we computed isotope ratios of each sample-standard comparison directly (i.e., naphthalene, phenanthrene and anthracene measurements for separate acquisitions of A0106). In some cases, A0106 was measured in series with a standard that was not well matched in concentration. In those cases, we multiplied the standard isotope ratio that was poorly matched with the sample (>2 orders of magnitude different) with a standard isotope ratio performed later that was well-matched with the standard. Errors for all ratios incorporated in this conversation were propagated in quadrature, which led in some cases (particularly, the $\delta^{13}C$ value for naphthalene in A0106) to be much larger than for measurements where sample-standard comparisons were performed more directly.

Tests of statistical significance

We performed tests of statistical significance on each of our measured $\Delta 2x^{13}C$ values for PAHs in both Ryugu sample C0107 and combusted plant samples to evaluate whether our measured values deviated significantly from predicted stochastic distribution ($\Delta 2x^{13}C = 0$). We formally tested null hypotheses H_0 against alternative two-sided hypotheses H_a where the mean of each measurement was significantly different from $\mu = 0$. *p*-values were reported based on

Welch's one-sample, one-sided *t*-tests using the "t.test" function in the R statistical software (www.r-project.org).

As reported in the Main Text, naphthalene, fluoranthene and pyrene values were found to be significantly different from $\mu = 0$ (where $H_0 > H_a$, and p-values were 1.159e-05, 0.003, and 0.001, respectively). Phenanthrene and anthracene values were not significantly different from $\mu = 0$ (where $H_0 = H_a$, and p-values were 0.16, and 0.45, respectively). $\Delta 2x^{13}C$ values of PAHs extracted from combusted plant samples are not significantly different from zero (p-values > 0.04; Table S3).

Reanalysis of Murchison $\delta^{13}C$ and $\Delta 2x^{13}C$ values from Zeichner et al., 2022

Murchison data were initially presented in the methods paper developing the direct elution method used herein (*33*). Murchison preparatory chemistry details can be found in (*33*). Since the time of publication, we have done additional studies using the GC-Orbitrap to measure low abundance samples and have discovered that it is imperative all scans incorporated in isotope analysis are performed under "AGC control," as mentioned above in "*Orbitrap mass spectrometry."* This was not the case for the data processed and presented in (*33*), so we reprocessed and represented the data here.

Murchison measurements were performed between December 2, 2016 and December 6, 2016 on the same instrument that was used for measurements of Ryugu and combusted plant biomass samples. 1-10pmol of each compound were measured per replicate injection, resulting in intensities ("NL scores") on the instrument of $5*10^6$ to $2*10^7$ per analysis.

The Murchison data was processed in the same way as the Ryugu data described above, with one difference: due to shifting elution times, each peak was integrated for a separate time window, where the length of the time frame integrated was kept consistent across all sample-standard comparisons (i.e., 30 seconds, even if the absolute start and end times varied; Table S2). Samples and standards were respectively averaged, and the quotient was taken to compute the ^{13}R value of the Murchison PAHs.

Murchison pyrene and fluoranthene $\delta^{13}C$ values were converted onto the VPDB scale by multiplying the values by the ^{13}R value of the terrestrial standards measured in comparison. The $\delta^{13}C_{VPDB}$ values of the fluoranthene and pyrene standards were measured in triplicate at Caltech by Elemental Analyzer (i.e., the same instrumentation as described above to constrain the $\delta^{13}C$ of the terrestrial standards used to constrain the Ryugu values), and were -25.69±0.46 and -25.68±0.66‰, respectively. Additional studies will be necessary to constrain δD values of these compounds in Murchison, the isotopic properties of the 2 and 3 ring PAHs in Murchison, and the isotopic compositions of PAHs of other carbonaceous chondrites for comparison.

Isotopic fractionation from mixing and other synthesis mechanisms

Mixing between two or more compound populations differing markedly in MA $\delta^{13}C$ values could create positive $\Delta 2x^{13}C$ anomalies. This is important to consider because large ranges in $\delta^{13}C_{VPDB}$ have been observed in prior studies of carbonaceous grains recovered from CCs (-950 to +36,000‰; (*71*)), which is evidence that these meteorites are mixed aggregates of pre-solar and early-solar-system materials differing in their stellar nucleosynthetic sources and post-formation processing. Mixing of two different formation processes with distinct isotopic signatures could create positive $\Delta 2x^{13}C$ values because predicted ^{13}C-clumping scales approximately with the square of the $^{13}C/^{12}C$ ratio, whereas mixing processes are approximately linear in plots of $\Delta 2x^{13}C$ vs. $\delta^{13}C$ (*19*). However, mixing would also be expected to lead to large

ranges in $\delta^{13}C$ values and correlations between $\delta^{13}C$ and $\Delta 2x^{13}C$ values, which we do not observe within the PAHs measured here (Table 1, Fig. 2). Instead, we favor a hypothesis where anomalies in multiple-^{13}C substitutions were generated by chemical or physical processes that controlled the state of isotopic ordering.

We acknowledge that excesses in $\Delta 2x^{13}C$ values of naphthalene, pyrene and fluoranthene from Hayabusa2 samples and fluoranthene from Murchison could be explained by a yet unrecognized isotopic fractionation associated with high temperature synthesis or reprocessing. Isotopic fractionation produced by shock wave chemistry in extraterrestrial environments is not thoroughly understood, but laboratory shock wave experiments producing diamond from graphite do not provide evidence for carbon isotope fractionations (*72*). Within the context of current research, we have not found evidence that any of these processes would explain the anomalous $2x^{13}C$-clumping observed in this samples measured in this study.

Density functional theory (DFT) model of acetylene equilibrium fractionation

Heavy isotope substitution slows fundamental modes of molecular vibration, reducing molecular vibrational energy and thus overall molecular free energy. This effect scales with reduced masses of molecular motions such that it is typically energetically favorable for molecules to assemble heavy rare isotopes (e.g., ^{13}C) into bonds with one another, rather than distributing them randomly across all possible atomic sites. In other words, it is energetically preferable for two molecules with C-C bonds to form one ^{12}C-^{12}C and one ^{13}C-^{13}C molecule versus two ^{13}C-^{12}C molecules. This isotopic clumping is reduced at higher temperatures due to the increasing importance of configurational entropy on overall free energy as temperature rises. Clumping is therefore expected to be indistinguishable from a stochastic distribution at temperatures greater than 300K. In cold environments, at temperatures below 100K, enrichments of double-heavy-isotope substitutions relative to a random distribution can exceed 10's of per-mille. Thus, the large positive $\Delta 2x^{13}C$ values of naphthalene, pyrene and fluoranthene may reflect chemical isotope effects in cold molecular clouds.

Acetylene (C_2H_2) is an abundant organic molecule in extraterrestrial environments, and is thought to be the precursor of organic molecules synthesized in many extraterrestrial environments. The distribution of ^{13}C in acetylene molecules versus free carbons, and in particular the doubly-substituted ^{13}C composition of acetylene can be represented by the equilibrium reaction (Eqn 1):

$$2 * {}^{13}C{}^{12}CH_2 \rightleftharpoons {}^{13}C_2H_2 + {}^{12}C_2H_2$$

where two free carbon-13 atoms substitute in for the two carbon-12 atoms within acetylene.

The distribution of isotopes in molecules within natural systems at equilibrium follows nonrandom probabilities, which provide a record of their sources, and synthesis histories (*19*). Symmetrically nonequivalent isotopic variations of a molecule create variations in all of its chemical and physical properties (e.g., vibrational energy, polarizability). This relationship can be described though the equilibrium partition function between isotopically substituted and unsubstituted molecules Q' and Q, in the Bigeleisen-Mayer model (BM model) as follows (*73*, *74*):

$$\frac{Q\prime}{Q} = \left[\left(\frac{m\prime}{m}\right)^{\frac{3r}{2}}\right]\left[\frac{\sigma}{\sigma\prime}\right]\prod\left[\frac{v_i\prime}{v_i} \times \frac{e^{\frac{-U_i\prime}{2}}}{e^{\frac{-U_i}{2}}} \times \frac{1-e^{\frac{-U_i}{2}}}{1-e^{\frac{-U_i\prime}{2}}}\right] \ (Eqn.S9),$$

where *m* is the mass of the unsubstituted isotope exchanged, m' is the mass of the substituted isotope exchanged, *r* is the # of atoms of the element of interest in the molecule, *σ and σ'* are the symmetry numbers of the unsubstituted and substituted molecules, *ν* and *ν'* are the frequency of the bond vibration in the unsubstituted and substituted versions of the molecule, and *Ui and Ui'* are the energies for each vibrational fundamental mode i of the unsubstituted and substituted molecules. *Ui* can be computed as follows:

$$U_i = \frac{h\nu_i}{k_B T} \ (Eqn. S10)$$

where h is Planck's constant, k_B is the Boltzmann constant, and T is temperature (K). *ν'/ ν* can be approximated by computing the square root of the ratio of the reduced masses:

$$\frac{\nu'}{\nu} = \sqrt{\frac{\mu}{\mu'}} \ (Eqn. S11)$$

Here, we used Density Functional Theory (DFT) to predict the optimal structure of acetylene molecule and calculate the fundamental vibrational modes of unsubstituted, singly-^{13}C substituted and doubly-^{13}C substituted acetylene *in vacuo*. These computations were performed with the B3LYP exchange correlation functional (*75*) and aug-cc-pVTZ basis set(*76*) using ENTOS Qcore simulation package (*77*). The aug-cc-pVTZ basis set has been previously found to be sufficiently large for convergence of equilibrium energy and structures of small organic compounds (*78*). The vibrational frequencies are then converted to reduced partition function ratios (RPFRs) using the BM model (Eqn. S9) with harmonic approximation. From these RPFRs, we can compute 1000*ln(sqrt($\frac{Q''}{Q} / \frac{Q'}{Q}$)), which is approximately the fractionation between the stochastic and the actual doubly-substituted ^{13}C composition for a δ^{13}C value at a given temperature (Fig. 2D). Notably, the fractionation is negligible at high temperatures, and can reach up to tens of per-mile at low temperatures (~10K).

Prior studies have raised concerns over the applicability of harmonic approximation and hence the validity of BM model at low temperature gas-phase conditions. Zhang and Liu suggested a series of corrections on BM model including (but not limited to) vibrational anharmonicity, rovibronic coupling, molecular rotations, centrifugal distortion diagonal Born-Oppenheimer correction (DBO) (*79*), which they demonstrated by computing the hydrogen isotope effects on several molecules with distinct geometries. The most important for our purposes seems to be DBO which relies on the premise that the Born-Oppenheimer approximation, inherent to the DFT calculations, breaks down due to correlation between nuclear and electronic motions at low temperatures. Such an approximation may have an effect on hydrogen, but (*79*) argues that the effect of such effects on heavier nuclides like C and O would be much smaller and most likely would not affect change our modelling results beyond analytical error. Here we set the DBO is equal to zero, as is the case for systems where reactants and products have identical wavefunctions (*80*).

The DFT model of isotopic clumping in acetylene yields an isotope effect that likely represents the maximum that could be recorded by a reversible chemical process in a molecule containing C-C bonds, both because it involves two heavy isotopes sharing a bond as nearest-neighbors, and because of the high order of the C-C bond in acetylene. Multiple substitutions separated by more bonds, and lower-order bonds between any given two elements tend to have

weaker clumping effects (*81*). If the PAHs were not exclusively derived from the addition of the 2-carbon units, then isotopic substitution could deviate from results from simple this model. This model is still appropriate for evaluating the amplitudes of clumped isotope anomalies that could arise through common chemical processes even if the reactants and products involved in PAH formation formed through irreversible reactions exhibiting kinetic isotope effects rather than the modeled equilibrium isotope reaction depicted in Eqn. 1 and Fig. 2D. Chemical kinetic isotope effects generally have amplitudes similar to equilibrium isotope effects (*20*), and so this model usefully demonstrates the order-of-magnitude of $2x^{13}C$ vibrational clumped isotope effects and their variations with temperature.

Table S1. **Background and blanks.** Serpentine blank and background quantification relative to intensity of sample peaks of interest for 8 Da windows direct elution measurements.

Mass window	**Compound**	**A0106** (NL score of base peak)	**A0106 background** (NL score of base peak)	**C0107** (NL score of base peak)	**C0107 background** (NL score of base peak)	**Serpentine blank** (NL score of base peak)
123.5-132.5	Naphthalene	5.29E5	4.49E3	2.60E5	3.75E3	3E3
173.5-182.5	Phenanthrene	2.95E5	3.63E3	6.68E4	3.70E3	6.42E2
	Anthracene	6.26E4	2.67E4	2.59E4	1.47E4	5.49E2
195.6 to 206.5	Fluoranthene	9.67E5	4.27E3	3.83E5	3.11E3	3.5E2
	Pyrene	3.30E6	7.62E3	1.25E6	5.22E3	3.45E2

Table S2. Experimental parameters for measurements of Ryugu samples, Murchison measurements and fire products. Each experiment lists the experimental parameters in the following order: mass window (MW; Da), time frame for peak integration (TF; minutes), AGC target (AGC), resolution (Res). Standards were measured in series with samples, under the exact same experimental conditions and data processing parameters. Dashes indicate that compound was not observed in a meaningful amount above baseline for that sample to measure.

Analysis month and year	Sample – Mass window (Injection volumes, sample/std)	Naphthalene				Phenanthrene				Anthracene				Fluoranthene				Pyrene			
		MW	TF	AGC	Res	MW	TF	AGC	Res	MW	TF	AGC	Res	MW	TF	AGC	Res	MW	TF	AGC	Res
April 2022	A0106 – 8Da (2.8µL/1.1µL)	124-132	20.7 – 22.15	$2*10^4$	120k	174-182	61.1 – 62.1	$2*10^4$	120k	174-182	62.1-63.35	$2*10^4$	120k	198-206	81.95-83.32	$1*10_5$	120k	198-206	85.3-87	$1*10^5$	120k
April 2022	C0107 – 8Da (2.5µL/0.6µL)	124-132	20.5-22.2	$2*10^4$	120k	174-182	61.2-62.4	$2*10^4$	120k	174-182	62.4-54	$2*10^4$	120k	198-206	81.95-83.32	$1*10_5$	120k	198-206	85.3-87	$1*10^5$	120k
April 2022	C0107 – 2 Da (4.5µL/1µL)	128.85-130.15	20.5 - 20.8	$2*10^4$	180k	178.85-180.15	61.13-61.8	$2*10^4$	180k	178.85-180.15	62.2-62.85	$2*10^4$	180k	202.85-204.15	82-83.05	$2*10_4$	180k	202.85-204.15	85.25-87	$2*10^4$	180k
Sept 2022	Marri ash – 8Da (1.1µL/1µL)	—	—	—	—	174-182	36.2-37.2	$1*10^5$	120k	—	—	—	—	198-206	55.85-57.5	$1*10_5$	120k	198-206	59.09-60.5	$1*10^5$	120k
Sept 2022	Marri ash – 2Da (1.1µL/1µL)	—	—	—	—	178.5-180.5	36.7-37.6	$2*10^4$	120k	—	—	—	—	202.5-204.5	56.9-58	$2*10_4$	120k	202.5-204.5	60.2-61	$2*10^4$	120k
Sept 2022	Cycads ash – 8Da (1µL/1.5µL)	—	—	—	—	174-182	36.7-37.6	$1*10^5$	120k	—	—	—	—	198-206	56.9-58	$1*10_5$	120k	198-206	60.2-61	$1*10^5$	120k
Sept 2022	Cycads ash – 2Da (1µL/1.5µL)	—	—	—	—	178.5-180.5	36.7-37.6	$2*10^4$	120k	—	—	—	—	202.5-204.5	56.9-58	$2*10_4$	120k	202.5-204.5	60.2-61	$2*10^4$	120k
Sept 2022	Gingko ash – 8Da (2µL/1µL)	—	—	—	—	174-182	36.7-37.6	$1*10^5$	120k	174-182	37.6-38.6	$1*10^5$	120k	198-206	56.9-58	$1*10_5$	120k	198-206	60.2-61	$1*10^5$	120k
Sept 2022	Gingko ash – 2Da (2µL/1µL)	—	—	—	—	178.5-180.5	36.7-37.6	$2*10^4$	120k	178.5-180.5	37.6-38.6	$2*10^4$	120k	202.5-204.5	56.9-58	$2*10_4$	120k	202.5-204.5	60.2-61	$2*10^4$	120k
Dec 2016	Murchison – 8Da (3µL/2µL)	—	—	—	—	—	—	—	—	—	—	—	—	198-206	32.98-33.36 (Murch 2), 32.88-33.26 (Murch 3), 32.85-33.23 (Murch 4), 32.86-33.24(Std 3), 32.82-33.2 (Std 4)	$2*10_5$	180k	198-206	34.5-32.93 (Murch 2), 34.3-34.73 (Murch 3 + 4), 34.37-34.8 (Std 3), 34.33-34.76 (Std 4)	$2*10^5$	180k

Table S3. Data from combusted plant samples. $\delta^{13}C_{VPDB}$ and $\Delta 2x^{13}C$ of phenanthrene, anthracene, fluoranthene and pyrene measured from C3 plants burned at different temperatures. $\delta^{13}C_{VPDB}$ values measured by the Orbitrap are compared to $\delta^{13}C_{VPDB}$ values measured by conventional compound specific isotope analysis methods and reported in (*50*). Reported σ are 1SE. Reported p-values (p-val) are results from one-sided t-tests evaluating significant differences between measured $\Delta 2x^{13}C$ values and the null hypothesis of $\Delta 2x^{13}C = 0$.

			phenanthrene				**anthracene**				**fluoranthene**				**pyrene**			
	T (C)		$\delta^{13}C$ value (VPDB, ‰)	σ	$\Delta 2x^{13}C$ (σ; ‰)	p-val	$\delta^{13}C$ value (VPDB, ‰)	σ	$\Delta 2x^{13}C$ (σ; ‰)	p-val	$\delta^{13}C$ value (VPDB, ‰)	σ	$\Delta 2x^{13}C$ (σ; ‰)	p-val	$\delta^{13}C$ value (VPDB, ‰)	σ	$\Delta 2x^{13}C$ (σ; ‰)	p-val
		this study	-28.1	*2.1*	-3.5 *(7.7)*	*0.58*	-24.1	*1.6*	-2.6 *(7.9)*	*0.46*	-24.2	*1.6*	-9.4 (7.5)	*0.12*	-30.4	*2.6*	10.8 (8.3)	*0.59*
gingko ash	142	Karp 2020	-27.7	*0.2*	-	-	-	-	-	-	-27.4	*0.1*	-	-	-27.6	*0.1*	-	-
		this study	-31.8	*2.7*	-3.6 *(8.5)*	*0.22*	-	-	-	-	-29.3	*2.7*	2.9 (7.3)	*0.28*	-31.7	*2.7*	7.2 (7.4)	*0.68*
cycads ash	594	Karp 2020	-26.8	*0.1*	-	-	-	-	-	-	-28.1	*0.1*	-	-	-26.8	*0.1*	-	-
		this study	-21.3	*2.5*	-12.5 *(7.7)*	*0.04*	-	-	-	-	-27.3	*2.5*	-0.2 (7.1)	*0.39*	-33.1	*2.6*	-3.1 (7.2)	*0.43*
marri ash	905	Karp 2020	-27.0	*0.7*	-	-	-	-	-	-	-27.3	*0.9*	-	-	-27.2	*0.6*	-	-

Table S4. Measurements of the $\delta^{13}C$ and $\Delta 2x^{13}C$ of fluoranthene and pyrene from Murchison. Results based on re-processing of data published in (*33*). $\delta^{13}C$ values from (*34*) are presented in the table alongside for comparison.

	Standard $\delta^{13}C$ value (*n*, **σ**; VPDB, ‰)	**Murchison $\delta^{13}C$ value** (*n*, **σ**; VPDB, ‰), this study	**Murchison Δ_{2x13C} (σ,** ‰), this study	**Murchison $\delta^{13}C$ value** (*n*, **σ**; VPDB, ‰), Gilmour and Pillinger, 1994
Fluoranthene	-25.69 (3, 0.46)	-9.9 (*3,* **1.0)**	51 (**13**)	-5.9 (**1.1**)
Pyrene	-25.63 (3, 0.66)	-11.3 (*3*, **1.1**)	1 (**13**)	-13.1 (**1.3**)

Table S5. Sensitivity tests for injection volume. Average isotope ratio and relative standard error (RSE = standard deviation/average, a proxy for error in ‰ units) for PAHs introduced as 1 and 5μL injections.

Compound	Injection Volume (μL)	Mass	Property measured	R value	Average	RSE
Pyrene	5	202	13C/UnSub	0.169929		
Pyrene	1	202	13C/UnSub	0.170139	0.170034	0.0006
Pyrene	5	202	2x13C/UnSub	0.012681		
Pyrene	1	202	2x13C/UnSub	0.012793	0.012737	0.0044
Fluoranthene	5	202	13C/UnSub	0.169789		
Fluoranthene	1	202	13C/UnSub	0.170018	0.169904	0.0007
Fluoranthene	5	202	2x13C/UnSub	0.012612		
Fluoranthene	1	202	2x13C/UnSub	0.012706	0.012659	0.0037
Naphthalene	5	128	13C/UnSub	0.107597		
Naphthalene	1	128	13C/UnSub	0.109210	0.108404	0.0074
Naphthalene	5	128	2x13C/UnSub	0.004860		
Naphthalene	1	128	2x13C/UnSub	0.005022	0.004941	0.0164
Anthracene	5	178	13C/UnSub	0.151578		
Anthracene	1	178	13C/UnSub	0.151142	0.151360	0.0014
Anthracene	5	178	2x13C/UnSub	0.010145		
Anthracene	1	178	2x13C/UnSub	0.010104	0.010124	0.0020
Phenanthrene	5	178	13C/UnSub	0.151314		
Phenanthrene	1	178	13C/UnSub	0.153305	0.152310	0.0065
Phenanthrene	5	178	2x13C/UnSub	0.009989		
Phenanthrene	1uL - jump method	178	2x13C/UnSub	0.010128	0.010058	0.0069

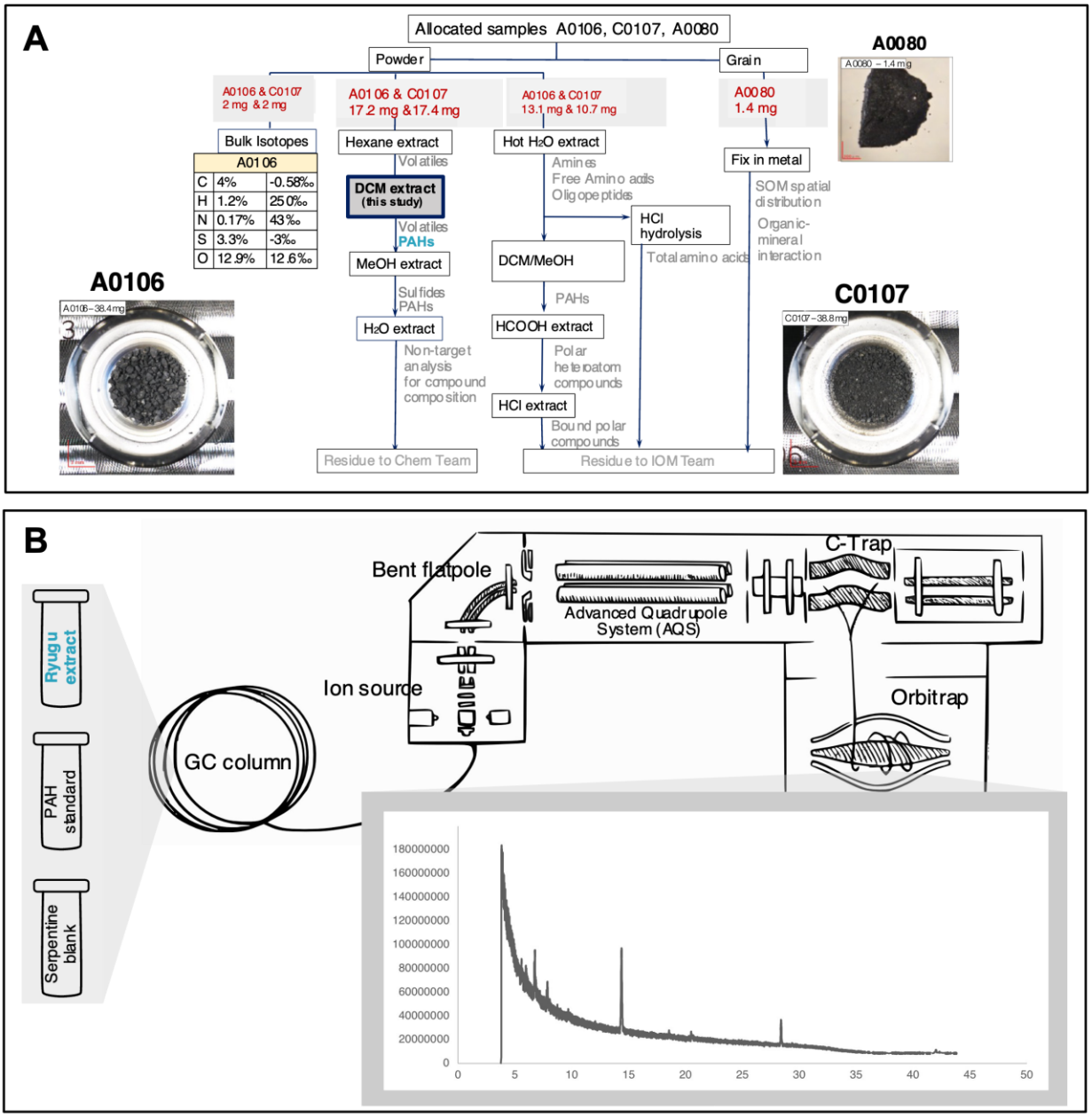

Figure S1. Methods. (**A**) Analytical scheme for Ryugu samples by the soluble organic matter team (*24*). DCM extracts of A0106 and C0107 were used in this study. (**B**) Ryugu extracts, PAH standards, and serpentine blanks were measured on the GC-Orbitrap at Caltech via direct elution method. (inset) Sample chromatogram from an injection of A0106, without mass jump. The majority of analyses were performed with the mass window jump method, where the Advanced Quadrupole System (AQS) is used to vary the mass window of interest throughout the run to perform focused measurements on each PAH of interest.

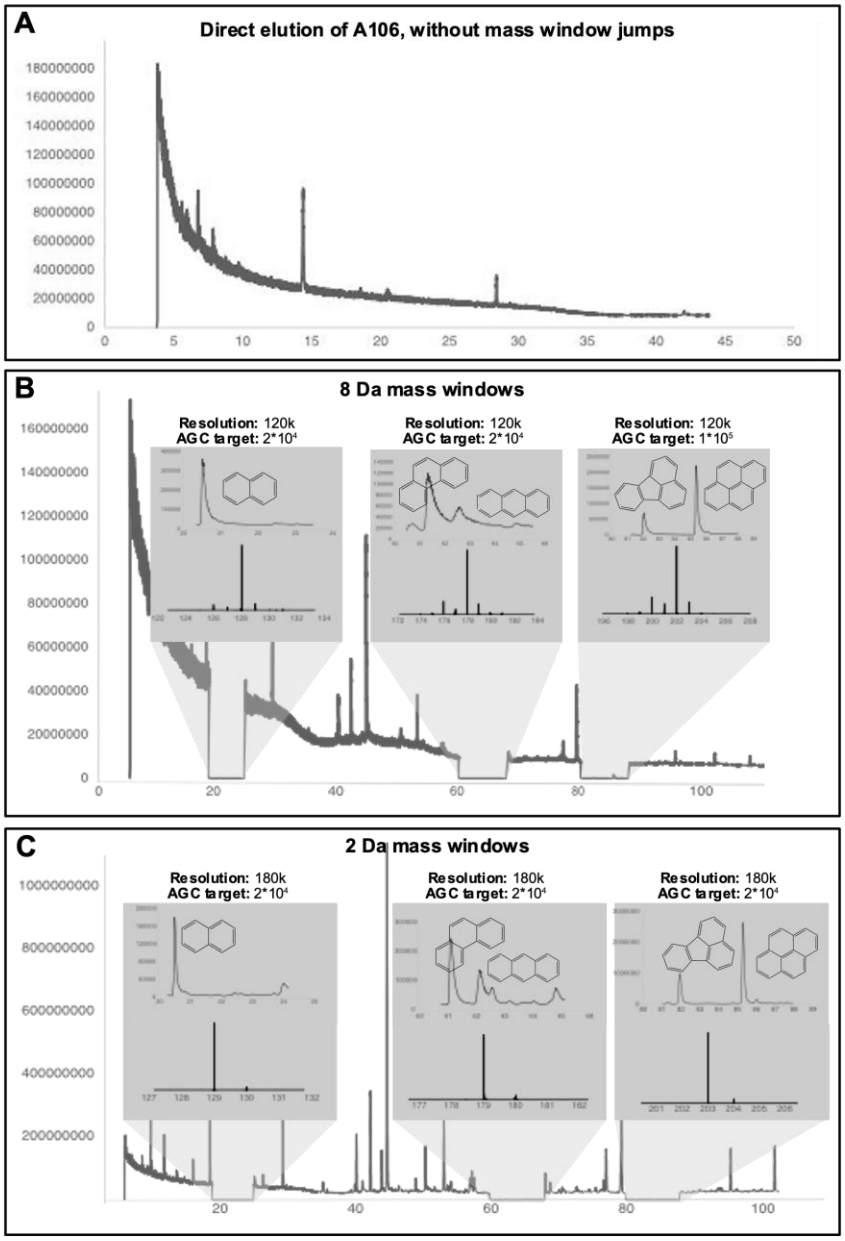

Figure S2. Chromatography. Direct elution method was used to measure 2, 3, and 4 ring PAHs from DCM extracts of Ryugu samples A0106 and C0107. (**A**) Initial measurement was performed without mass window jumping; subsequent measurements were performed with focused (**B**) 8 Da and (**C**) 2 Da windows. For each mass window, both the chromatogram and the mass spectrum for one of the Ryugu sample measurements is shown, annotated with the molecular structure of the PAH of the eluting peak.

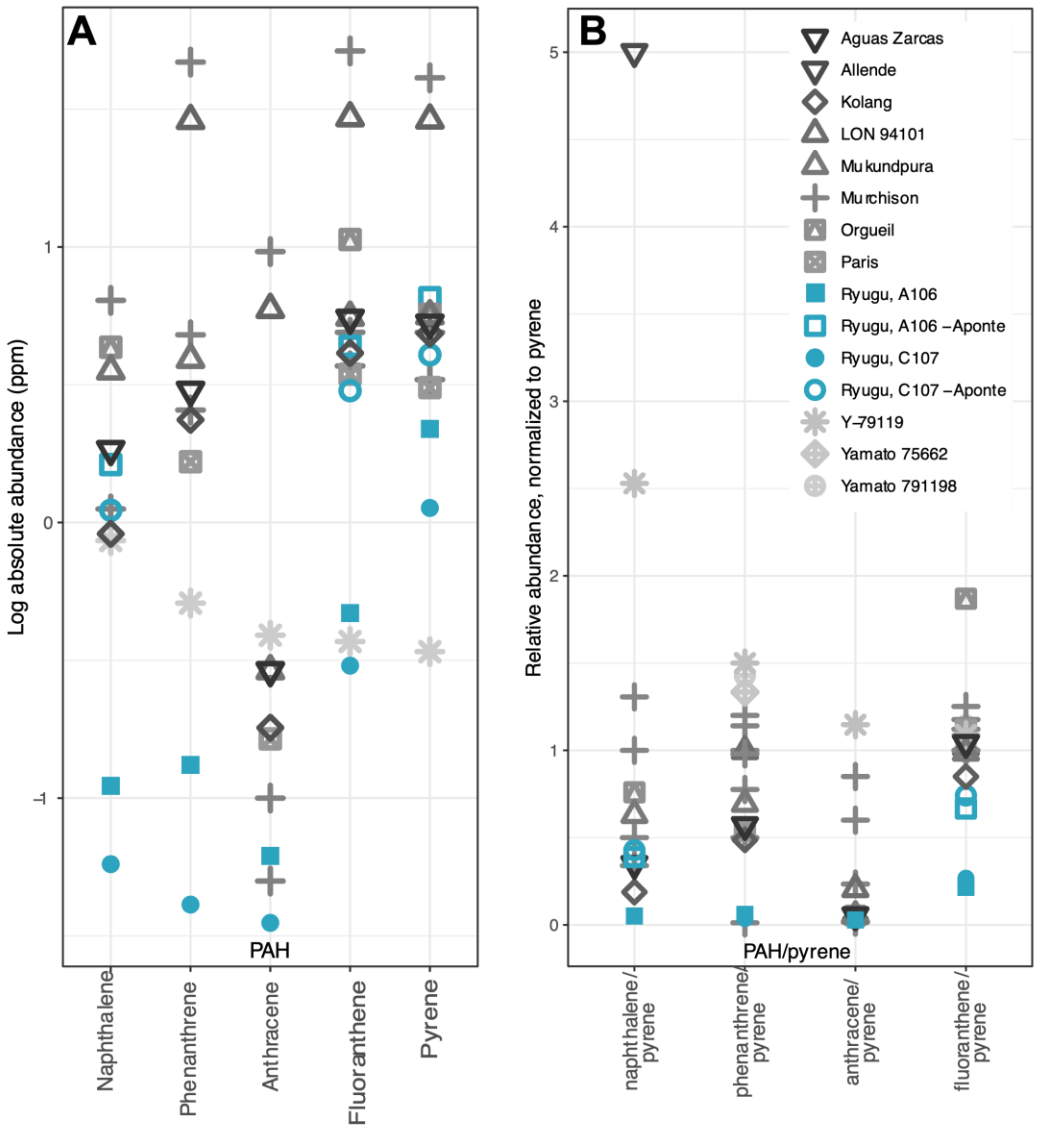

Figure S3. Absolute and relative abundances. (**A**) Log absolute abundances of 2, 3, and 4 ring PAHs in units of ppm (μg/g) extracted from Ryugu samples A0106 and C0107 measured in this study (filled cyan squares and circles) and (*32*) (unfilled black squares and circles), compared to prior quantifications of abundances of PAHs in extracts of other meteorite samples (grey symbols). (**B**) Relative abundances of 2, 3, and 4 ring PAHs normalized to the abundance of pyrene, for extracts of measured in this study (filled cyan squares and circles) and (*32*) (unfilled black squares and circles) and other meteorite samples (grey symbols). Abundance measurements come from the following references: (*34*, *58–60*, *64*, *65*, *82–89*).

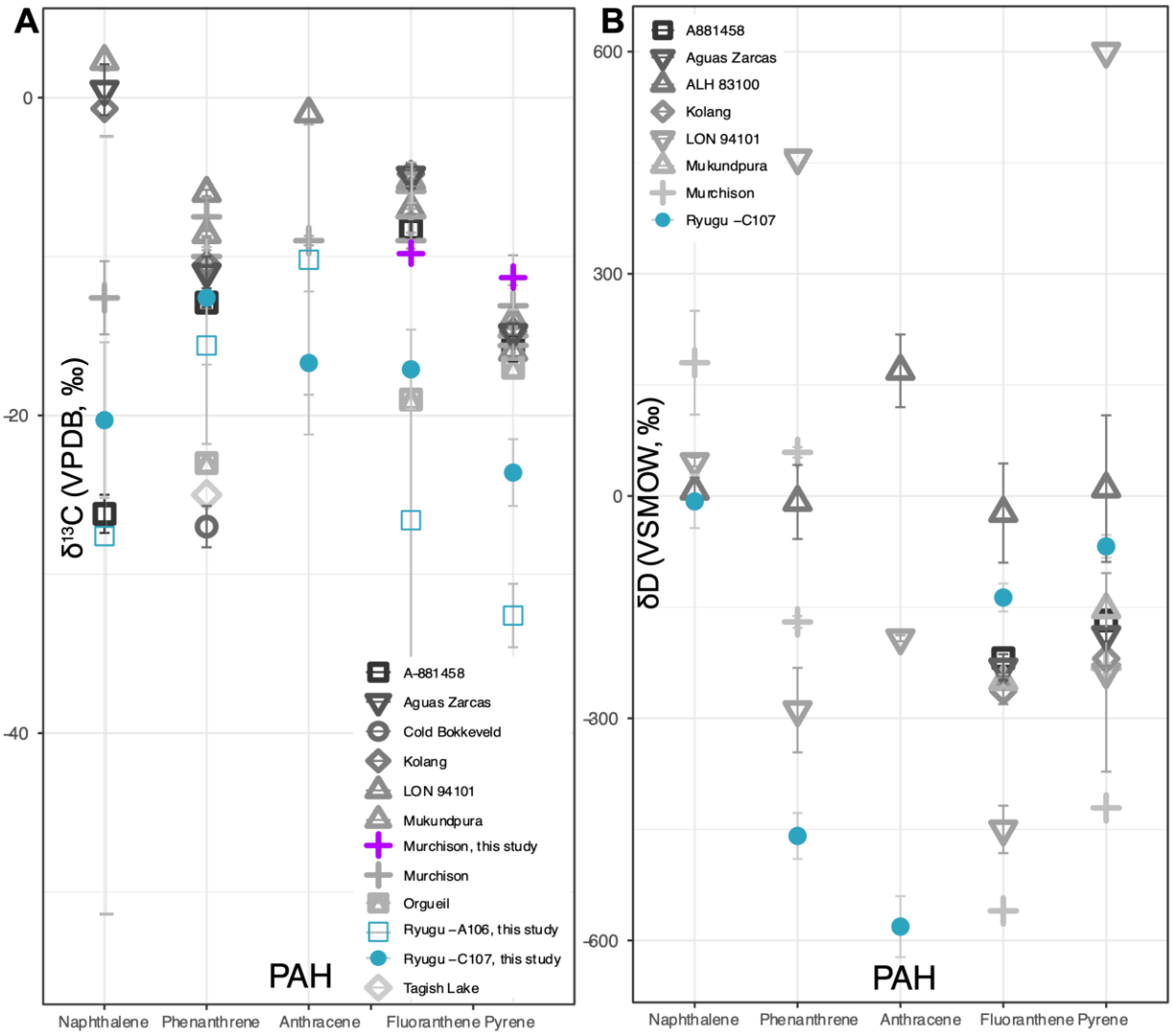

Figure S4. δ^{13}C and δD values. Measured (**A**) δ^{13}C values (A0106 = unfilled cyan squares, C0107 = filled cyan circles, Murchison = purple plus signs) and (**B**) δD values of Ryugu PAHs (filled cyan circles) via direct elution measurement on the GC-Orbitrap, compared with prior measurements of PAHs extracted from meteorites (grey symbols). Compiled prior measurements are from the following studies: (*34*, *64–68*, *89*, *90*).

Mode no.	Vibrational frequency, ν (cm^{-1})			
	Unsubstituted	Single ^{13}C	Double ^{13}C	
	Anti-symmetric C-H bending			
1	665.40	660.32	655.33	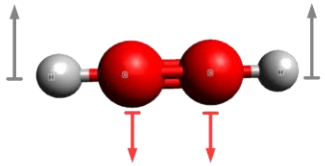
2	665.44	660.42	655.37	
	Symmetric C-H bending			
3	768.43	767.34	766.15	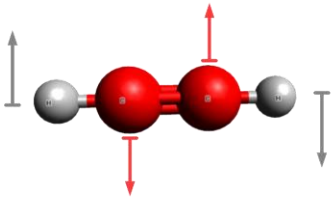
4	768.49	767.40	766.21	
	Symmetric C-C stretching			
5	2064.73	2032.36	1999.03	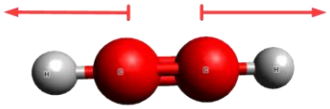
	Anti symmetric C-H stretching			
6	3408.25	3402.62	3398.16	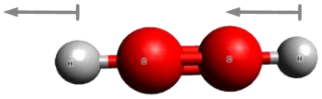
	Symmetric C-H stretching			
7	3512.97	3500.56	3487.20	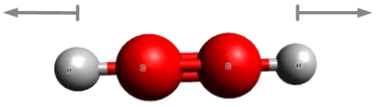

Figure S5. Vibrational modes. The fundamental vibrational modes of acetylene along with their corresponding motions calculated using B3LYP/aug-cc-pVTZ level of DFT. Modes 1,2 and 3,4 are doubly degenerate.

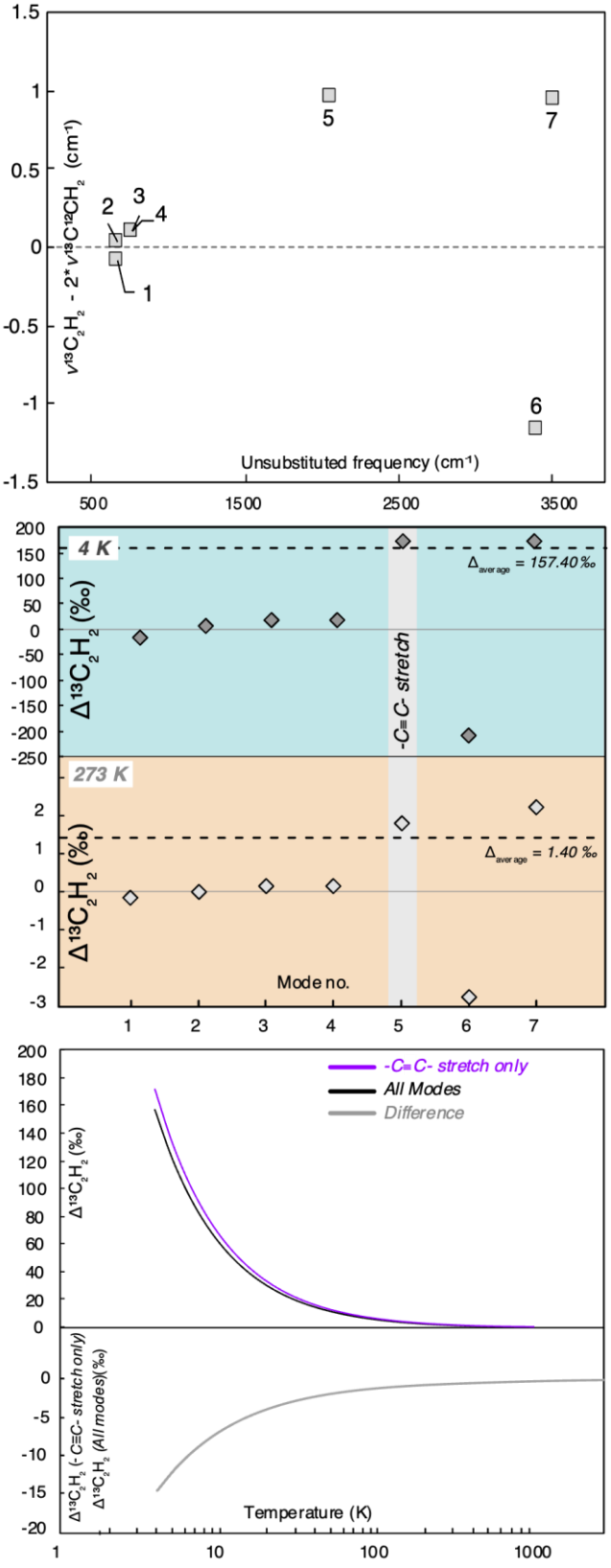

Figure S6. Effect of modes on ^{13}C-clumping. The effect of different modes in contribution to the overall double ^{13}C substitution clumped isotope effect of acetylene. (**top**) The shift of fundamental mode frequency (in cm^{-1}) on double ^{13}C substitution for different modes (numbers correspond to mode numbers included in Figure S5). Note that the high frequency modes (5, 6, 7) have higher frequency shift. (**middle**) The contribution of each fundamental mode towards calculation of $\Delta^{13}C_2H_2$. Note that higher frequencies contribute the most and the average effect considering all modes fall close to the one calculated using C-C stretch only. The upper panel and the lower panel demonstrate the same phenomena at different temperatures (4K and 273K). (**bottom**) Temperature dependence of the $\Delta^{13}C_2H_2$ calculated using all modes and C-C stretch only. The difference between them is demonstrated on the lower panel.